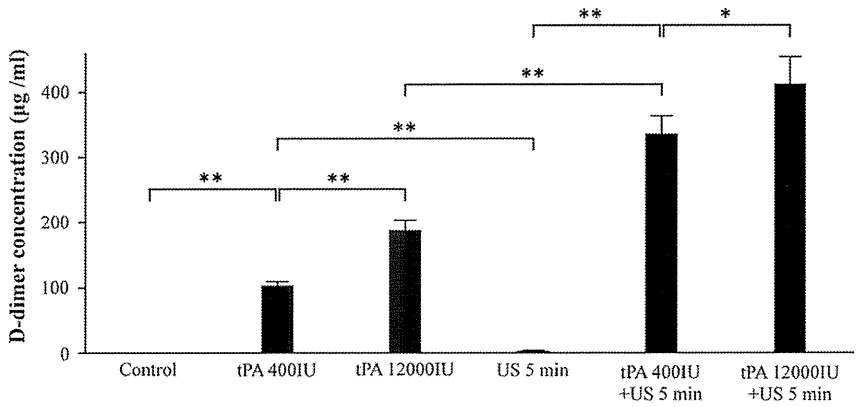

Fig. 2. Amount of D-dimer after US exposure and tPA. D-dimer was increased by tPA in a dose dependent fashion. Simultaneous US exposure and tPA significantly increased the amount D-dimer (paired *t*-test, $*p < 0.05$, $**p < 0.01$).

change in temperature from 37°C after US exposure in all experiments.

Effects of US and tPA. D-dimer was significantly increased by tPA application and also showed a dose-dependent effect (Fig. 2, $p < 0.01$). Because 5 min exposure was sufficient to obtain treatment effects, the following US exposure times were fixed for 5 min. As a result, D-dimer was increased by tPA in a dose-dependent fashion. Simultaneous US exposure and tPA significantly increased D-dimer (Fig. 2).

Safety of US exposure. With a 6 mm probe, $I_{SPPA.3}$ was less than 28 W/cm^2 but the derated spatial-peak temporal-average intensity ($I_{SPTA.3}$) was far more than 17 mW/cm^2 in all conditions. With a 3 mm probe, $I_{SPPA.3}$ was less than 28 W/cm^2 and $I_{SPTA.3}$ was also less than 17 mW/cm^2 under the condition of a duty cycle of 5.2%. All computed acoustic parameters were referred in Table 1.

In vivo study

Sonothrombolysis. Before US irradiation, the fibrin score was approximately 2.4 and there were no statistical differences between groups. In the controls, intracameral fibrin clot decreased gradually over time, and the average score on day 3 was 1.4 ± 0.21. While eyes that received subconjunctival tPA injection alone showed a slight decrease of clots, and the average score was 1.2 ± 0.19. There was no statistically significant difference with controls. In contrast, eyes that received US alone or both subconjunctival tPA and US showed apparent decreases of clots and the average scores decreased to 0.75 ± 0.13 and 0.71 ± 0.11, respectively (control vs. US alone; $p < 0.05$ and control vs. US with subconjunctival tPA; $p < 0.01$) (Figs. 3 and 4). During the experimental course, no pathologic change such as edema or new bleeding was observed in any of cornea, anterior chamber, iris or lens by surgical microscopic observation (Fig. 4).

Ocular surface temperature. Before US exposure, the surface temperature was approximately 25°C (less than 32 °C in the periocular area) (Fig. 5A). Immediately after US exposure, the temperature started to increase. Under the US condition: frequency of 1.0 MHz, duty cycle of 5.2%, pulse repetition frequency of 20 Hz and $I_{SPPA.3}$ of 0.228 W/cm^2, the temperature increased slightly (approximately 28.5°C) and always remained less than about 32°C in the periocular area (Fig. 5B). However,

Table 1. Acoustic output level of ultrasounds about Sonitron 2000

Probe	Intensity (Indicated on the device)	Duty cycle	Pulse repetition frequency	Peak rarefactional acoustic pressure (MPa)	$I_{SPPA.3}$ (W/cm^2)	$I_{SPTA.3}$ (mW/cm^2)
6 mm	Low mode	5.2%	20 Hz	0.397	5.409	280.169
6 mm	Low mode	100%	continuous wave	0.425	5.982	5933.022
6 mm	High mode	5.2%	20 Hz	0.545	10.123	524.369
6 mm	High mode	100%	continuous wave	0.575	11.220	11128.540
3 mm	Low mode	5.2%	20 Hz	0.070	0.177	9.190
3 mm	Low mode	100%	continuous wave	0.065	0.155	154.032
3 mm	High mode	5.2%	20 Hz	0.083	0.228	11.791
3 mm	High mode	100%	continuous wave	0.062	0.156	154.484
FDA safety regulation					<28	<17

The frequency of this machine was fixed 1.0 MHz. $I_{SPPA.3}$ was less than 28 W/cm^2 under all conditions. Meanwhile $I_{SPTA.3}$ was less than 17 mW/cm^2 under only the condition of a duty cycle of 5.2% with 3 mm probe.

$I_{SPPA.3}$ = a derated spatial-peak pulse-average intensity; $I_{SPTA.3}$ = a derated spatial-peak temporal-average intensity.

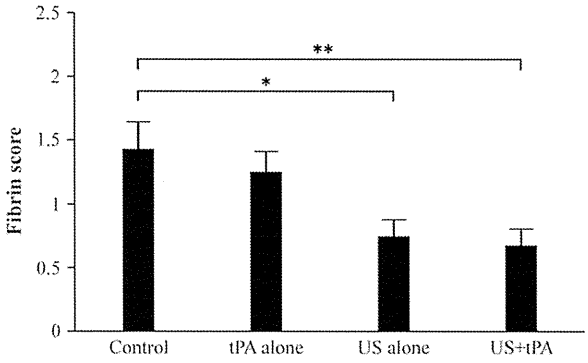

Fig. 3. Intracameral fibrin score on day 3. Intracameral fibrin clot decreased gradually over time and the average score on day 3. While the eyes that received subconjunctival tPA injection alone showed mild decrease of clots. There was no statistically significant difference from controls. In contrast, the eyes that received US alone or both tPA and US showed apparent decrease of clots (paired *t*-test, $*p < 0.05$, $**p < 0.01$).

under the US condition: frequency of 1.0 MHz, duty cycle of 100%, continuous wave mode and $I_{SPPA.3}$ of 0.156 W/cm^2, the temperature increased considerably (to about 34°C) more than the periocular area (Fig. 5C).

Histological findings. In immediate histological finding after YAG laser treatment, there was not any apparent damage in other ocular tissues including cornea and retina (Fig. 6). After US irradiation, the structure of the cornea was well preserved and neither inflammatory cell infiltration nor stromal edema was found. Retinal structure was also well preserved and neither inflammatory infiltrate nor hemorrhage was observed either (Fig. 7).

DISCUSSION

In this study, we found that US exposure significantly accelerated the disappearance of intracameral fibrin without causing any apparent damage. It is further important that this effect was accomplished within the range of safety condition.

Many reports show that US exposure accelerates fibrinolysis in vitro and combining US with various thrombolytic agents, *e.g.*, heparin sulfate, aspirin, urokinase type-plasminogen activator or tPA further accelerated fibrinolysis (Francis et al. 1992; Holland et al. 2008; Hong et al. 1990; Lauer et al. 1992; Tachibana 1992; Trübestein et al. 1976). In the present study, US exposure significantly enhanced fibrinolysis *in vitro* without thermal elevation; this effect was augmented by tPA. Although we cannot know the exact mechanism by which US accelerated fibrinolysis, most currently accepted or possible explanations are that US exposure changes the structure of clots and alters the drug distribution, resulting in deeper penetration into the clots by US, namely due to acoustic cavitations, bubble vibration, and their collapse (Datta et al. 2006; Francis et al. 1992; Hong et al. 1990; Lauer et al. 1992; Tachibana 1992; Trübestein et al. 1976). Of note, we have to interpret the results cautiously. In this study, we used borosilicate glass

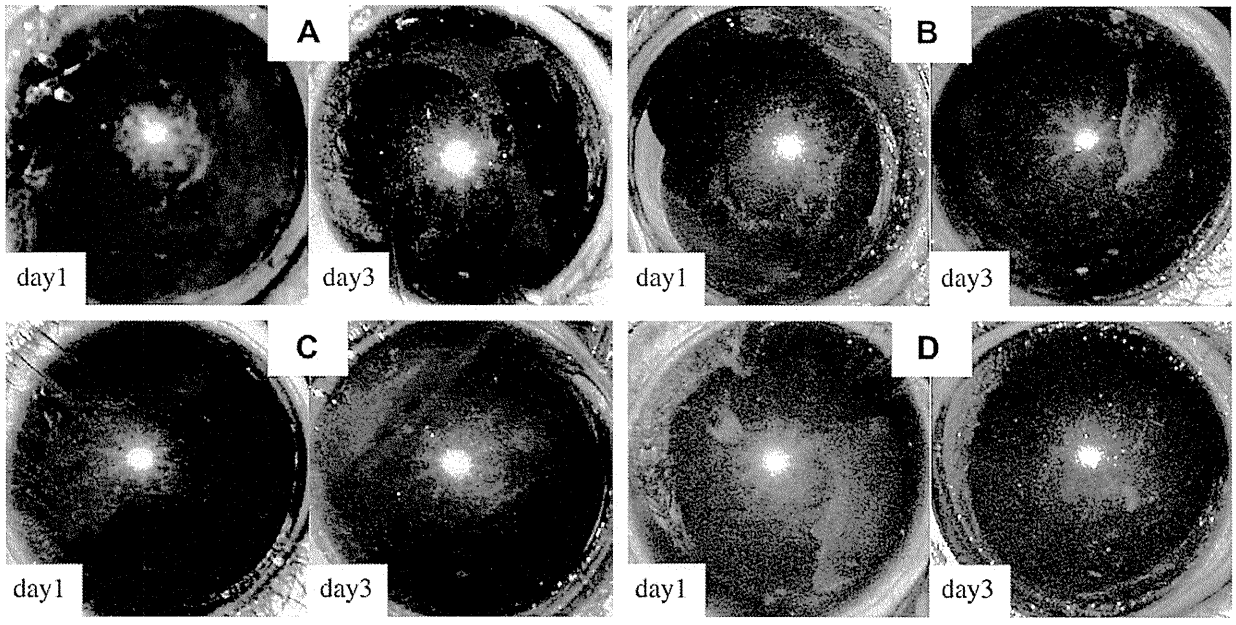

Fig. 4. Representative photograph of rat eyes after bleeding followed by treatment. Intracameral bleeding was induced by Nd:YAG laser shot on iris followed by subconjunctiva tPA injection and/or US exposure. Intracameral fibrin was scored on day 3. (A) Control. Fibrin clots decreased gradually. (B) US exposure alone. Fibrin clots was apparently decreased. (C) Subconjunctival tPA injection alone. Fibrin clots decreased gradually and there was no apparent difference from controls. (D) Subconjunctival tPA plus US exposure. Fibrin clots was significantly decreased and no clot was observed on day 3.

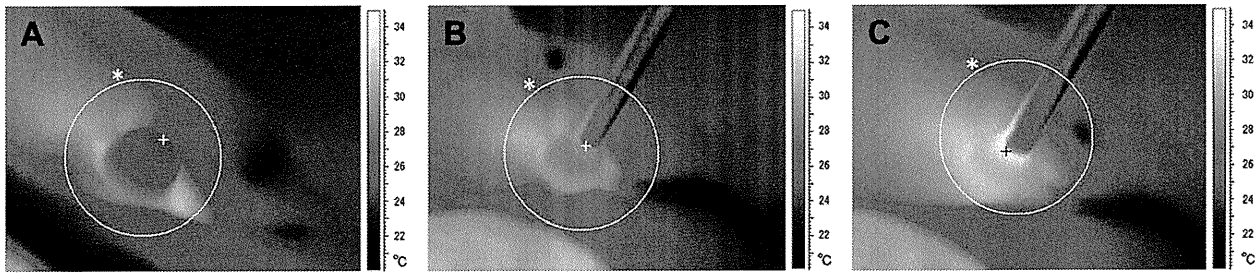

Fig. 5. The thermographic images of ultrasound-treated eye by an infrared thermography. Temperature was expressed as a pseudo-color. (A) Control. The highest temperature within the circle (denoted by an asterisk) was 31.9°C and the temperature of the spot + was 24.4°C. (B) US exposure for 5 min under the condition: frequency of 1.0 MHz, duty cycle of 5.2%, pulse repetition frequency of 20 Hz and $I_{SPPA.3}$ of 0.228 W/cm^2. The highest temperature within the circle (denoted by an asterisk) was 31.2°C and the temperature of the spot + was 28.5°C. (C) US exposure for 5 min under the condition: frequency of 1.0 MHz, duty cycle of 100%, continuous wave mode and $I_{SPPA.3}$ of 0.156 W/cm^2. The highest temperature within the circle (denoted by an asterisk) was the area of the spot +, which was 33.7°C.

tubes and that might have augmented ultrasound effect excessively. The unexpected reflection might have been involved in this phenomenon. However, it was unlikely that the present fibrinolysis was caused by thermal effect, because there was no change in temperature in the tube before and after ultrasound in this in vitro system even by the prolonged exposure (20 min). Importantly, the goal of our study is clinical application of US for intraocular fibrinolysis, which could be achieved in rat eyes. It requires further studies to elucidate the real mechanism of the present phenomenon.

Heating is a concern for tissue damage but it could accelerate clot-lysis on the other hand. Francis et al. (1992, 1995) reported that US exposure is associated with only a minimal increase of clot temperature even at 4 W/cm^2, which would be more potent than our conditions. In this study, the clot temperature *in vitro* shows less increase under the condition: frequency of 1.0 MHz, duty cycle of 5.2%, pulse repetition frequency of 20 Hz and $I_{SPPA.3}$of 10.123 W/cm^2 and the ocular surface temperature *in vivo* showed a minimal increase under the condition: frequency of 1.0 MHz, duty cycle of 5.2%, pulse repetition frequency of 20 Hz and $I_{SPPA.3}$ of 0.228 W/cm^2. Thus, it is likely that a nonthermal mechanism played a central role in our observations. Given the results of the *in vitro* study, it is understandable that intracameral fibrinolysis was accelerated by US exposure in rats. However, *in vivo* conditions are totally different from those *in vitro*.

In our previous study using the same model, there were various pro- or antifibrinolytic materials in the anterior chamber such as tPA and its inhibitor, unlike in vitro experiments (Sakamoto et al. 1999). Additionally, the intraocular environment is not stable and is strongly modulated by other factors. For example, if severe inflammation occurred, intracameral fibrin was easily formed while intracameral fibrin disappeared after the inflammation had gone. On the other hand, platelets were reported to be activated *in vitro* by US exposure (Chater and Williams 1977). Thus, it was of note that US exposure under the present condition caused fibrinolysis in the present study.

Under normal conditions, anterior chamber fluid is transparent and tPA is dominant over plasminogen

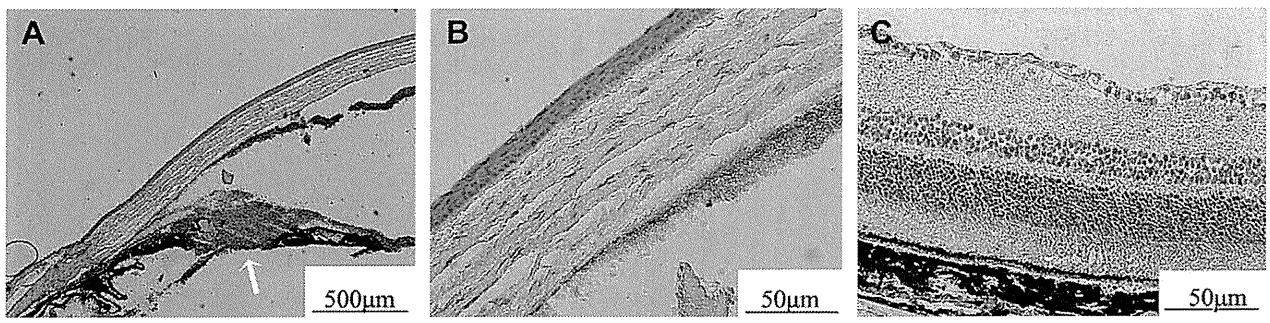

Fig. 6. Histologic photographs of rat eyes after YAG laser shot, before US exposure. (A) The only limited area of iris (arrow) was destroyed, called iridectomy hole, and 1/3 of the anterior chamber was filled with fibrin clot and red blood cells. (B) Fibrin clot and fibrin deposit were also found just beneath the corneal endothelium. There was not any apparent damage in other ocular tissues including cornea (B) and retina (C). Hematoxylin and eosin staining. Original magnification is (A) ×4, (B) ×40 and (C) ×40.

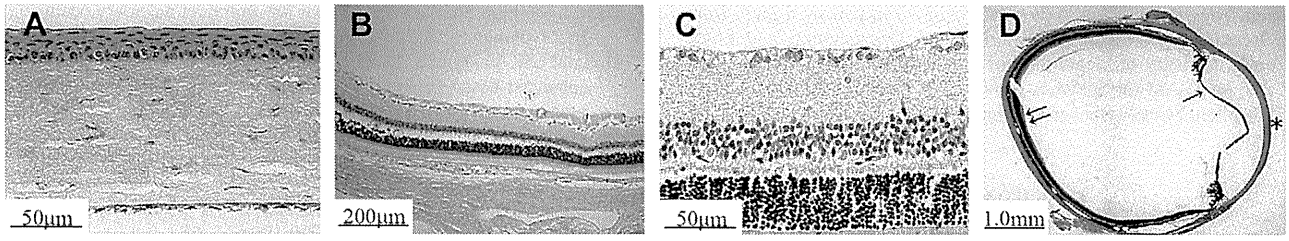

Fig. 7. Histologic photographs of rat eyes after US exposure. Original structure is well preserved and neither degeneration nor inflammation is found in cornea (A), retino-choroid (B) or retina (C). (D) The eyeball of the rat. Asterisk indicates cornea, arrow indicates iris and double arrow indicates retina. Hematoxylin and eosin staining. Original magnification is (A) ×40, (B) ×4, (C) ×40 and (D) ×2.

activator inhibitor (Fukushima et al. 1989). Fibrinolytic materials such as tPA were also assumed to be dominant over inhibitors after iris bleeding in this model because intracameral fibrin decreased gradually without any treatment. Therefore, US treatment accelerated intracameral fibrinolysis associated with tPA to some extent. Further study is necessary to clarify the mechanism in more detail.

Unlike the *in vitro* study, the additional injection of tPA to US exposure did not augment intracameral fibrinolysis. In this study, we did not use a direct intraocular injection of tPA because the intraocular injection itself could influence the intraocular fibrinolytic system. Instead, tPA was injected into subconjunctiva to avoid this destabilizing factor. As a result, it could not further enhance fibrinolysis. It was possible that subconjunctival tPA was degraded or did not penetrate the anterior chamber and thus active tPA might not be present sufficiently in the anterior chamber. An improved drug delivery system would be necessary.

US is a routine diagnostic procedure for ocular diseases and therapeutic application to glaucoma and intraocular tumor has already reported (Coleman et al. 1985, 1988). US is also believed to be a promising therapeutic alternative by several experimental studies (Sonoda et al. 2006; Yamashita et al. 2007; White et al. 2008; Zderic et al. 2004). However, US has still not been accepted for clinical use in most of ocular diseases including intraocular hemorrhage and vascular disorders.

This is not only because therapeutic value has not been well developed but there have also been concerns about its potentially harmful effects (Brown 1984). For example, the corneal endothelium *in vitro* was damaged by US exposure (Saito et al. 1999).

As this study reveals, the effects of US were influenced by various factors. Among them, the duty ratio was the strongest factor inducing a possible harmful event. In our *in vivo* study, the surface temperature of rat eyes increased to about 34 °C with the following conditions: frequency of 1.0 MHz and duty cycle of 100%, which was higher than periocular area while the surface temperature was not changed so much with a duty cycle of 5.2%. It is difficult to conclude that the present treatment is not harmless; however, it should be noted that a beneficial effect, intracameral fibrinolysis, could be obtained without causing a harmful event, histologically or clinically. Obviously, a human eye is much bigger than a rat eye and careful setting of US conditions would enable the therapeutic value of this treatment to be established.

There are many ocular diseases to which this treatment is potentially applicable. Of them, RAO is a good candidate. As is often quoted, a disease without any treatment has many treatments and RAO is a good example. The onset-to-treatment interval is the most critical issue for the successful treatment of RAO because longer periods of tissue ischemia result in irreversible retinal damage and permanent dysfunction. In a study with primates, the interval should be less than a few hours (Hayreh 2008; Hayreh et al. 2004). In comparison to surgery or intraocular injection, the present treatment is less invasive and does not need specific preparations for treatment (*e.g.*, disinfection treatment), which might waste precious time for effective treatment. Furthermore, US exposure might also be effective for removing cholesterol or calcium emboli because US can induce mechanical vibration. Considering these benefits, the present treatment should be worthy of study in a future clinical setting, although there are still many issues to be solved.

It is of note that our animal model is not that of retinal artery occlusion. To our knowledge, there is no reproducible animal model of retinal artery occlusion that is suitable for evaluating therapies. In contrast, the present model is suitable for studying the effect of intervention on intraocular fibrinolysis *in vivo*. This would give us the important information to develop a new treatment of retinal artery occlusion.

In conclusion, the present study shows that US exposure from outside can accelerate intraocular fibrinolysis. A beneficial effect was obtained without causing apparent damage. The US power was within the safety range of FDA regulations. Therefore, there might be more suitable ocular conditions for US treatment than given in the examples above. The present results could provide basic evidence to justify US treatment for ocular diseases related to fibrin formation.

Acknowledgements—This study was supported in part by a grant from the Research Committee on Chorioretinal Degeneration and Optic Atrophy, Ministry of Health, Labor and Welfare (Dr. Sakamoto) and by a Grant-in-Aid for Scientific Research 19659452 from the Ministry of Education, Science and Culture, Japanese Government, Tokyo, Japan.

REFERENCES

Akassoglou K, Adams RA, Bauer J, Mercado P, Tseveleki V, Lassmann H, Probert L, Strickland S. Fibrin depletion decreases inflammation and delays the onset of demyelination in a tumor necrosis factor transgenic mouse model for multiple sclerosis. Proc Natl Acad Sci U S A 2004;101:6698–6703.

Alexandrov AV, Molina CA, Grotta JC, Garami Z, Ford SR, Alvarez-Sabin J, Montaner J, Saqqur M, Demchuk AM, Moye LA, Hill MD, Wojner AW. Ultrasound-enhanced systemic thrombolysis for acute ischemic stroke. N Engl J Med 2004;351:2170–2178.

Brown BS. How safe is diagnostic ultrasonography? Can Med Assoc J 1984;131:307–311.

Chater BV, Williams AR. Platelet aggregation induced *in vitro* by therapeutic ultrasound. Thromb Haemost 1977;38:640–651.

Cohen MG, Tuero E, Bluguermann J, Kevorkian R, Berrocal DH, Carlevaro O, Picabea E, Hudson MP, Siegel RJ, Douthat L, Greenbaum AB, Echt D, Weaver WD, Grinfeld LR. Transcutaneous ultrasound-facilitated coronary thrombolysis during acute myocardial infarction. Am J Cardiol 2003;92:454–457.

Coleman DJ, Lizzi FL, Driller J, Rosado AL, Burgess SE, Torpey JH, Smith ME, Silverman RH, Yablonski ME, Chang S, Rondeau MJ. Therapeutic ultrasound in the treatment of glaucoma. II. Clinical applications. Ophthalmology 1985;92:347–353.

Coleman DJ, Silverman RH, Iwamoto T, Lizzi FL, Rondeau MJ, Driller J, Rosado A, Abramson DH, Ellsworth RM. Histopathologic effects of ultrasonically induced hyperthermia in intraocular malignant melanoma. Ophthalmology 1988;95:970–981.

Daffertshofer M, Gass A, Ringleb P, Sitzer M, Sliwka U, Els T, Sedlaczek O, Koroshetz WJ, Hennerici MG. Transcranial low-frequency ultrasound-mediated thrombolysis in brain ischemia: Increased risk of hemorrhage with combined ultrasound and tissue plasminogen activator: Results of a phase II clinical trial. Stroke 2005;36:1441–1446.

Datta S, Coussios C-C, McAdory LE, Tan J, Porter T, de Courten-Myers G, Holland CK. Correlation of cavitation with ultrasound enhancement of thrombolysis. Ultrasound Med Biol 2006;32:1257–1267.

Drake MV. Neodymium:YAG laser iridotomy. Surv Ophthalmol 1987;32:171–177.

Feltgen N, Neubauer A, Jurklies B, Schmoor C, Schmidt D, Wanke J, Maier-Lenz H, Schumacher M. Multicenter study of the European Assessment Group for Lysis in the Eye (EAGLE) for the treatment of central retinal artery occlusion: Design issues and implications. EAGLE Study report no. 1: EAGLE Study report no. 1. Graefes Arch Clin Exp Ophthalmol 2006;244:950–956.

Francis CW, Onundarson PT, Carstensen EL, Blinc A, Meltzer RS, Schwarz K, Marder VJ. Enhancement of fibrinolysis *in vitro* by ultrasound. J Clin Invest 1992;90:2063–2068.

Francis CW, Blinc A, Lee S, Cox C. Ultrasound accelerates transport of recombinant tissue plasminogen activator into clots. Ultrasound Med Biol 1995;21:419–424.

Frenkel V, Oberoi J, Stone MJ, Park M, Deng C, Wood BJ, Neeman ZM III, Li KC. Pulsed high-intensity focused ultrasound enhances thrombolysis in an *in vitro* model. Radiology 2006;239:86–93.

Fukushima M, Nakashima Y, Sueishi K. Thrombin enhances release of tissue plasminogen activator from bovine corneal endothelial cells. Invest Ophthalmol Vis Sci 1989;30:1576–1583.

Garcia-Arumi J, Martinez-Castillo V, Boixadera A, Fonollosa A, Corcostegui B. Surgical embolus removal in retinal artery occlusion. Br J Ophthalmol 2006;90:1252–1255.

Hayreh SS, Zimmerman MB, Kimura A, Sanon A. Central retinal artery occlusion. Retinal survival time. Exp Eye Res 2004;78:723–736.

Hayreh SS. Intra-arterial thrombolysis for central retinal artery occlusion. Br J Ophthalmol 2008;92:585–587.

Holland CK, Vaidya SS, Datta S, Coussios C-C, Shaw GJ. Ultrasound-enhanced tissue plasminogen activator thrombolysis in an *in vitro* porcine clot model. Thromb Res 2008;121:663–673.

Hong AS, Chae JS, Dubin SB, Lee S, Fishbein MC, Siegel RJ. Ultrasonic clot disruption: An *in vitro* study. Am Heart J 1990;120:418–422.

Jaffe GJ, Schwartz D, Han DP, Gottlieb M, Hartz A, McCarty D, Mieler WF, Abrams GW. Risk factors for postvitrectomy fibrin formation. Am J Ophthalmol 1990;109:661–667.

Kattah JC, Wang DZ, Reddy C. Intravenous recombinant tissue-type plasminogen activator thrombolysis in treatment of central retinal artery occlusion. Arch Ophthalmol 2002;120:1234–1236.

Lauer CG, Burge R, Tang DB, Bass BG, Gomez ER, Alving BM. Effect of ultrasound on tissue-type plasminogen activator-induced thrombolysis. Circulation 1992;86:1257–1264.

McDonald HR, Schatz H, Johnson RN. Postoperative intraocular fibrin formation is a potentially disastrous complication of vitrectomy surgery. Retina 1990;10:317–318.

Noble J, Weizblit N, Baerlocher MO, Eng KT. Intra-arterial thrombolysis for central retinal artery occlusion: A systematic review. Br J Ophthalmol 2008;92:588–593.

Opremcak E, Rehmar AJ, Ridenour CD, Borkowski LM, Kelley JK. Restoration of retinal blood flow *via* translumenal Nd:YAG embolysis/embolectomy (TYL/E) for central and branch retinal artery occlusion. Retina 2008;28:226–235.

Pfaffenberger S, Devcic-Kuhar B, Kastl SP, Huber K, Maurer G, Wojta J, Gottsauner-Wolf M. Ultrasound thrombolysis. Thromb Haemost 2005;94:26–36.

Richard G, Lerche RC, Knospe V, Zeumer H. Treatment of retinal arterial occlusion with local fibrinolysis using recombinant tissue plasminogen activator. Ophthalmology 1999;106:768–773.

Saito K, Miyake K, McNeil PL, Kato K, Yago K, Sugai N. Plasma membrane disruption underlies injury of the corneal endothelium by ultrasound. Exp Eye Res 1999;68:431–437.

Sakamoto T, Oshima Y, Nakagawa K, Ishibashi T, Inomata H, Sueishi K. Target gene transfer of tissue plasminogen activator to cornea by electric pulse inhibits intracameral fibrin formation and corneal cloudiness. Hum Gene Ther 1999;10:2551–2557.

Sonoda S, Tachibana K, Uchino E, Okubo A, Yamamoto M, Sakoda K, Hisatomi T, Sonoda KH, Negishi Y, Izumi Y, Takao S, Sakamoto T. Gene transfer to corneal epithelium and keratocytes mediated by ultrasound with microbubbles. Invest Ophthalmol Vis Sci 2006;47:558–564.

Tachibana K. Enhancement of fibrinolysis with ultrasound energy. J Vasc Intervent Radiol 1992;3:299–303.

Tachibana K, Tachibana S. Albumin microbubble echo-contrast material as an enhancer for ultrasound accelerated thrombolysis. Circulation 1995;92:1148–1150.

Tachibana K, Tachibana S. Prototype therapeutic ultrasound emitting catheter for accelerating thrombolysis. J Ultrasound Med 1997;16:529–535.

Tomey KF, Traverso CE, Shammas IV. Neodymium-YAG laser iridotomy in the treatment and prevention of angle closure glaucoma. A review of 373 eyes. Arch Ophthalmol 1987;105:476–481.

Toth CA, Morse LS, Hjelmeland LM, Landers MB III. Fibrin directs early retinal damage after experimental subretinal hemorrhage. Arch Ophthalmol 1991;109:723–729.

Trubestein G, Engel C, Etzel F, Sobbe A, Cremer H, Stumpff U. Thrombolysis by ultrasound. Clin Sci Mol Med Suppl 1976;3:697s–698s.

Vine AK, Samama MM. The role of abnormalities in the anticoagulant and fibrinolytic systems in retinal vascular occlusions. Surv Ophthalmol 1993;37:283–292.

Weber J, Remonda L, Mattle HP, Koerner U, Baumgartner RW, Sturzenegger M, Ozdoba C, Koerner F, Schroth G. Selective intra-arterial fibrinolysis of acute central retinal artery occlusion. Stroke 1998;29:2076–2079.

White WM, Makin IR, Slayton MH, Barthe PG, Gliklich R. Selective transcutaneous delivery of energy to porcine soft tissues using Intense Ultrasound (IUS). Lasers Surg Med 2008;40:67–75.

Yamamoto T, Kamei M, Kunavisarut P, Suzuki M, Tano Y. Increased retinal toxicity of intravitreal tissue plasminogen activator in a central

retinal vein occlusion model. Graefes Arch Clin Exp Ophthalmol 2008;246:509–514.

Yamashita T, Sonoda S, Suzuki R, Arimura N, Tachibana K, Maruyama K, Sakamoto T. A novel bubble liposome and ultrasound-mediated gene transfer to ocular surface: RC-1 cells in vitro and conjunctiva *in vivo*. Exp Eye Res 2007;85:741–748.

Yoeruek E, Spitzer MS, Tatar O, Biedermann T, Grisanti S, Luke M, Bartz-Schmidt KU, Szurman P. Toxic effects of recombinant tissue plasminogen activator on cultured human corneal endothelial cells. Invest Ophthalmol Vis. Sci 2008;49:1392–1397.

Zderic V, Clark JI, Vaezy S. Drug delivery into the eye with the use of ultrasound. J Ultrasound Med 2004;23:1349–1359.

OA0812-05

多波長分光画像による眼底酸素飽和度の計測

＝眼底網膜機能の直接評価のための分光学的アプローチ＝

九州大学　中村　大輔・吉永　幸靖
岡田　龍雄・石橋　達朗
九州医療センター　江内田　寛

1．はじめに

近年、緑内障や糖尿病網膜症等による中途失明が増加しており、眼底病変の早期発見や予防的治療法の開発が望まれている。現在の眼底疾患の診断には蛍光眼底造影法や走査型レーザ検眼鏡などを用いた侵襲の多い網脈絡膜血流動態の検査や、OCT（Optical Coherence Tomography）などの形状計測技術が主に利用されているが、疾患部位における定量診断や疾患メカニズムの解明のためには血糖値や酸素飽和度、たんぱく質といった網膜機能情報の直接評価が有効であると考えられる。中でも酸素飽和度は糖尿病網膜症などの眼底疾患との関連性があると言われており、さらに眼底疾患以外の脳や心臓の疾患の診断の指標値としても注目されている。酸素飽和度はパルスオキシメータに代表されるように分光分析手法を利用することで計測することができる。分光分析によるヒトの眼底酸素飽和度計測は1963年にHickamらによってなされて以来[1]、より高い信頼性を目指して多くの研究者により計測法の開発が試みられてきた[2]~[10]。しかし、眼底組織層における光反射の複雑さや眼底形状による反射光の変動および眼底組織内に存在する色素や固視微動といった問題が高精度な酸素飽和度計測の妨げとなっている。本稿では、本研究にて新たに提案した多波長分光イメージングと画像処理を利用した眼底酸素飽和度計測法について紹介し、眼底の酸素飽和度計測結果について述べる。

2．眼底酸素飽和度計測法

血液中に存在するヘモグロビンは酸素の結合状態によって分光特性が異なる。したがって、2波長以上の分光計測を行なうことで酸素飽和度を計測することが可能となる。パルスオキシメータでは一般に赤色、近赤外光が利用されるが、ヘモグロビンは図1に示すように500～600 nmの領域において特徴的な高い吸光特性を有するため[11]、本研究では550 nm帯の波長を用いることとした。測定においては近赤外光の方が視覚への負担が低いが、緑色光の方が網膜表面部のみからの反射光を捕らえることができる利点を有する。実験ではヘモグロビンの酸素結合に依存しない545 nmと依存する560 nmの2波長を用いた。

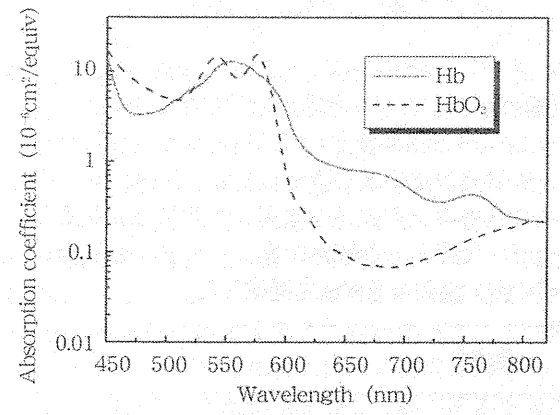

図1　ヘモグロビンの吸光度特性

図2に眼底網膜部の断面モデルを示す。本研究では、計測に用いる緑色光は網膜色素上皮（rpe：Retinal pigment epithelium）よりも下層にある脈絡膜などからの反射は無視できるほど小さいと仮定した。図2に示すように血管部からの反射光をI_{in}、血管部近傍の血管外からの反射光をI_{out}とすると、2つの反射光の違いは血管部における吸収もしくは散乱のみと見なすことができるため光学密度（OD：Optical density）は次式で表される。

0917-026X/09/¥500/論文/JCLS

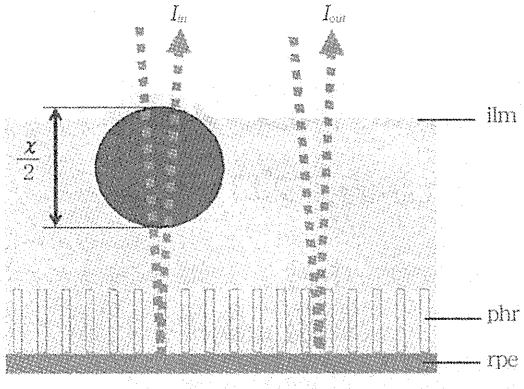

図2　網膜部の断面モデル
内境界膜（ilm：Inner limiting membrane）から網膜色素上皮間の網膜部は視細胞（phr：Photoreceptors）を含め透明と仮定。

$$OD = \log_{10}\left(\frac{I_{out}}{I_{in}}\right) = ax \qquad \cdots(1)$$

ここで、aはヘモグロビンの減衰係数である。網膜色素上皮細胞には分光特性を有するメラニン色素が存在するが、隣接する部分では一様に分布していると仮定するとODではその影響は消える。さらに、計測波長である545、560 nmの光学密度比（ODR：OD ratio）は次式で表される。

$$ODR = \frac{OD_{560}}{OD_{545}} = \frac{a_{560} \cdot x}{a_{545} \cdot x} = \frac{a_{560}}{a_{545}} \qquad \cdots(2)$$

したがって、ODRは減衰係数のみに関係する値となる。酸素飽和度はこのODRと線形相関があることから[7]、本研究でもODRを指標値として用いる手法を採用した。さらに、本研究では眼底表面形状や固視微動の影響を抑えるために2台のCCDカメラを用いた同時分光計測とモルフォロジー演算および線集中度フィルターを組み合わせた網膜の酸素飽和度計測法を提案した。

3．実験

眼底計測のための光学系にはトプコン社製の眼底カメラ（TRC 50IA、Topcon Co.、Japan）を用いて、光源には眼底カメラ内蔵のXeフラッシュランプを利用した。2波長画像を同時計測するために図3に示すようなビームスプリッタと2台のEM-CCDカメラ（ADT-40S-KM1、Flovel Co.、Ltd.、Japan）から成る計測系を眼底カメラに取り付けた。2台のCCDカメラの手前にはそれぞれ545、560 nmの干渉フィルター（$\Delta\lambda$=3.7、4.3 nm）を取り付けることで2波長同時計測を行なった。

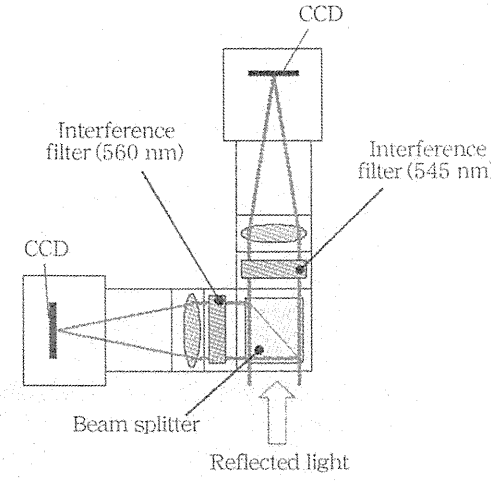

図3　眼底画像計測系の構成図

4．実験結果

4－1　2波長画像同時計測

実験において健康な20代男性を被験者とし、眼底撮影を行なった。図4に本実験装置を用いて2波長（545、560 nm）同時撮影した眼底画像を示す。これらの画像はフラッシュランプ照射のタイミングに合わせて撮影された。中央にある輝度の高い部分が視神経乳頭部であり、そこから血管が四方へ走っているのが確認できる。

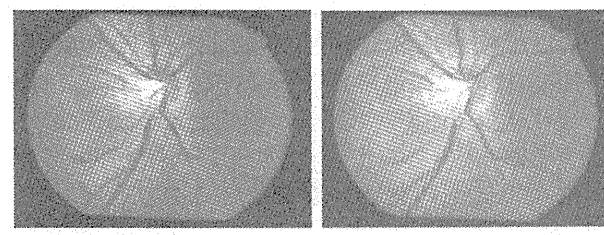

(a) 545 nm　　(b) 560 nm

図4　2波長同時計測した眼底画像

4－2　I_{out}の推定

この2画像からそれぞれの血管部のODを算出するにあたり、前述したような血管構造検出により血管部と隣接する血管外部を選択する手法に替えて、本研究ではモルフォロジーのClosing演算を用いて血管以外からの反射光I_{out}を推定する手法を適用した。取得した画像において黄斑部や視神経乳頭部の表面形状に起因する反射光強度や網膜色素上皮に存在するメラニン色素分布は、血管部の反射光強度に対して充分緩やかであると仮定できる。これは、胃X線二重造影像と似ており[12]、円盤を構造要素と

して用いたClosing演算を行なうことで画像全体の反射光I_{out}を見積もることができる。図５に構造要素の半径を15pixelとしたときの画像を示す。図４の画像と比較すると図５では血管部のみが除かれたような画像になっていることがわかる。したがって、この画像を用いることで血管部の局所的なODだけでなく画像全体のODを導出することができ、545、560 nmそれぞれの画像からODRマップの算出が可能となる。構造要素の半径は血管太さに対応させる必要があるが、血管径の半値程度に設定値を調整することで反射光I_{out}を推定することが可能となる。

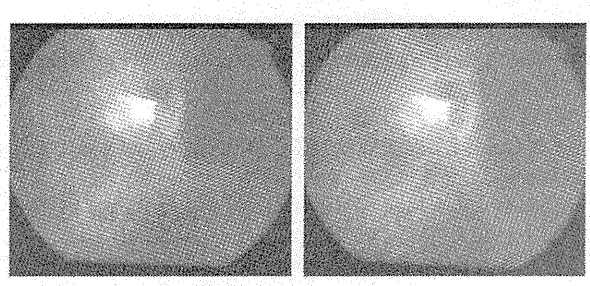

(a) 545 nm　　(b) 560 nm

図５　Closing演算後の画像

４－３　血管抽出

Closing演算による反射光I_{out}の推定では血管辺縁等など演算前とほぼ同値となる箇所が存在することとなる。このため式(1)は非常に小さな値となり、式(2)において計算誤差が無視できない状況になる。そこで、血管部のみを対象とするため血管を抽出する必要がある。Closing演算前と後で値の差が大きな点を血管部と見なすことも可能であるが、本研究ではコントラストに依存しない線検出法である線集中度フィルターを利用して血管抽出を行なった[13]。これは、画像における輝度勾配ベクトルを求め、ベクトルの方向のみに着目してその集中度を利用する演算手法である。図６に図４(a)の画像において線集中度フィルターを用いて血管抽出を行なった結果を示す。この図より太い血管だけでなく枝分かれした淡く細い血管部も抽出できていることが確認できる[14]。

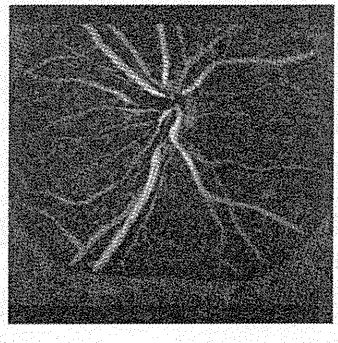

図６　線集中度フィルターにより血管抽出を行なった画像

４－４　酸素飽和度マップの算出

同時計測した２波長画像に対して前述したClosing演算と線集中度フィルターを用いた演算を行なうことで、酸素飽和度の指標値であるODRマップを算出することができる。図７に算出したODR画像を示す。式(2)からわかるようにODRの値が高い方が酸素飽和度が低く、ODRの値が低い方が酸素飽和度が高くなる。図７ではODRの値に対して色分けを施しており、色が黒くなるほど酸素飽和度が低いことを表している。血管ごとに色の違いがあることが確認できるが、眼科医の所見の結果、解剖学的知識による動静脈の分類とほぼ一致した。したがって、本手法により血管太さ50 μm程度以上の血管について動静脈の識別できることが確認された。

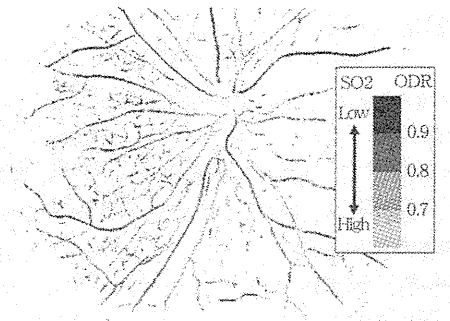

図７　酸素飽和度の指標値であるODR画像

４－５　無呼吸時の酸素飽和度モニタリング

次に、酸素飽和度の変動に対する本手法の性能を評価するため、無呼吸時における眼底酸素飽和度のモニタリングを行なった。まず、無呼吸時にどのような酸素飽和度の変化を示すかを耳部に取り付けたパルスオキシメータ（Rad-5、Masimo Co.、USA）により計測した。被験者に約80秒間息を止めてもらい、測定した結果、0～50秒まではほぼ100%を維持し、60秒前後から徐々に酸素飽和度が低下しはじめ、80秒前後で約80%程度までほぼ線形に酸素飽和度が低下することがわかった。３回測定を行なったが、いずれの場合も同等の結果であった。耳部と眼底は肺からの距離がほぼ等しく血中酸素飽和度の変化も同等であると仮定し、無呼吸時の眼底酸素飽和度を計測した。評価には図４(a)にて画像中央上部に併走している動脈と静脈を用いた。図８に無呼吸時における耳部の酸素飽和度に対する分光画像より算出したODRの値を示す。この結果より動静脈ともに耳部で計測した酸素飽和度の変動に対応してODRの値が変化していることがわかる。この結果は、ODRが酸素飽和度をモニタリングしていることを示唆しており、我々は本手法が眼底酸素飽和度をモニタリングできる潜在的な能力を有すると推測している。

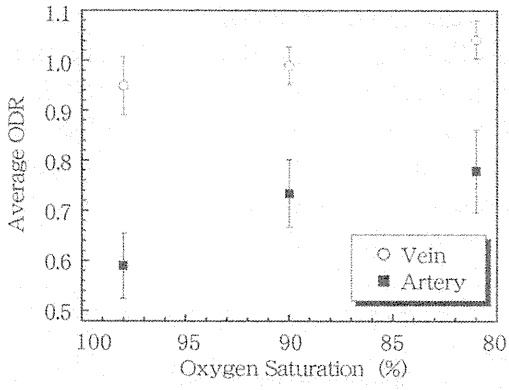

図8　無呼吸時におけるODRの変動

5．おわりに

545、560 nmの2波長同時分光計測とClosing演算および線集中度フィルターを組み合わせた網膜の酸素飽和度計測法を提案し、眼底酸素飽和度マップを算出した。その結果、動静脈の識別が可能であることを確認し、無呼吸時の酸素飽和度のモニタリングについても評価を行なった。一方、本手法で算出した血管部のODR値のばらつきが大きいため、今後、信頼性を高める必要がある。現在考えられるばらつきの原因として、取得する2画像のわずかな位置ズレや回転ズレ、および眼球レンズの歪みによる局所的なフォーカスのズレなどが挙げられる。これらは、画像の補正処理精度の向上や補償光学系を用いることで改善できると推測される。また、本手法では無視しているが血管壁による反射によって血管中央の反射強度が高くなる現象もODR値ばらつきの要因の一つであると考えられる。その他改善の余地は充分に考えられるが、本手法が眼底酸素飽和度計測の潜在的な能力を有していると推測する。さらに、現在は次段階としてハロゲンランプを光源としEM-CCDカメラを用いた2波長ビデオレート分光計測による酸素飽和度モニタリングを試みている。ビデオレート撮影により拍動する血管の様子が確認されており、酸素飽和度の動画計測が期待される。

謝辞

本研究は、九州大学教育研究プログラム研究拠点形成プロジェクト「安心で健全な高齢者のベターライフを目的とした新しい検診・診断システムの構築」の援助による。

〈参考文献〉

(1) Hickam JB, Frayser R, Ross J. C., Circulation. 27, 375 (1963)
(2) T. T. J. M. Berendschota, P. J. DeLintb, D. v. Norren, Prog. Retin. Eye Res. 22, 171 - 200 (2003)
(3) F. C. Delori, Appl. Opt. 27, 6, 1113 (1988)
(4) M. H. Smith, K. R. Denninghoff, L. W. Hillman, and R. A. Chipman, J. Biomed. Opt. 3, 3, 296 - 303 (1998)
(5) B. Khoobehi, J. M. Beach, and H. Kawano, Invest. Ophthalmol. Vis. Sci. 45, 5, 1464 (2004)
(6) M. Ito, K. Murayama, T. Deguchi, M. Takasu, T. Gil, M. Araie, G. Peyman, S. Yoneya, Exp. Eye Res. 86, 512 (2008)
(7) J. M. Beach, K. J. Schwenzer, S. Srinivas, D. Kim, J. S. Tiedeman, J. Appl. Physiol. 86, 748 (1999)
(8) S. H. Hardarson, A. Harris, R. A. Karlsson, G. H. Halldorsson, L. Kagemann, E. Rechtman, G. M. Zoega, T. Eysteinsson, J. A. Benediktsson, A. Thorsteinsson, P. K. Jensen, J. Beach, E. Stefsson, Invest. Ophthalmol. Vis. Sci. 47, 5011 (2006)
(9) H. Arimoto, H. Furukawa, Proc. of IEEE EMBS, 1627 (2007)
(10) J. C. Ramella-Roman, S. A. Mathews, H. Kandimalla, A. Nabili,D. D. Duncan, S. A. DiAnna, S. M. Shah, Q. D. Nguyen, Opt. Exp. 16, 6170 (2008)
(11) O. W. Van Assendelft, Royal Vangorcum, ch. 3, 47 (1970)
(12) 福島重廣・渡利靖子・吉永幸靖：電子情報通信学会、技術報告、MI2002－51、25（2002）
(13) 吉永幸靖・小畑秀文・福島重廣・縄野繁：電子情報通信学会論文誌、J87-D-II、146（2004）
(14) 吉永幸靖・山根大・末田聡・松岡昇・中村大輔・岡田龍雄・館眞利・江内田寛・石橋達朗：第7回情報科学フォーラム論文集（第2分冊）、35（2008）

【筆者紹介】

中村大輔
九州大学　大学院　システム情報科学研究院
電子システム工学部門　准教授
〒839-0395　福岡市西区元岡744
TEL／FAX：092-802-3679

吉永幸靖
九州大学　大学院　芸術光学研究院　芸術情報部門
情報環境学講座　助教
〒815-8540　福岡市南区塩原4-9-1
TEL／FAX：092-553-4571

岡田龍雄
九州大学　大学院　システム情報科学研究院
電子システム工学部門　教授
〒839-0395　福岡市西区元岡744
TEL／FAX：092-802-3695

石橋達朗
九州大学　大学院　医学研究院　臨床医学部門　眼科学分野
教授
〒812-8582　福岡市東区馬出3-1-1
TEL：092-642-5645　FAX：092-642-5663

江内田　寛
(独)国立病院機構　九州医療センター　眼科医長
〒810-8563　福岡市中央区地行浜1-8-1
TEL：092-852-0700　FAX：092-847-8802

Experimental Eye Research 88 (2009) 92–98

Contents lists available at ScienceDirect

Experimental Eye Research

journal homepage: www.elsevier.com/locate/yexer

Asymmetry of focal macular photopic negative responses (PhNRs) in monkeys

Yukihide Kurimoto [a], Mineo Kondo [a,*], Shinji Ueno [a], Takao Sakai [a], Shigeki Machida [b], Hiroko Terasaki [a]

[a] Department of Ophthalmology, Nagoya University Graduate School of Medicine, 65 Tsuruma-cho, Showa-ku, Nagoya 466-8550, Japan
[b] Department of Ophthalmology, Iwate Medical University School of Medicine, Morioka, Japan

ARTICLE INFO

Article history:
Received 26 August 2008
Accepted in revised form 15 October 2008
Available online 1 November 2008

Keywords:
electroretinogram
photopic negative response (PhNR)
asymmetry
macula
focal
monkey

ABSTRACT

The photopic negative response (PhNR) is a slow, negative-going wave of the photopic electroretinogram (ERG) that appears after the b-wave. Recent studies have shown that the PhNR originates from the spiking activities of inner retinal neurons including the ganglion cells and their axons. The aim of this study was to determine whether there is any asymmetry in the amplitude of the PhNR elicited from the upper and lower macular areas, and between the nasal and temporal macular areas in rhesus monkeys. To accomplish this, we recorded focal macular PhNRs that were elicited by red hemi-circular stimuli presented on a blue background. We show that the PhNR from the upper macular area was significantly larger than that of the lower macular area, and the PhNR of the nasal macula was significantly larger than that of the temporal macula. These asymmetries were present in the focal PhNR elicited by both brief and long duration stimuli, and the asymmetries were completely eliminated by an intravitreal injection of tetrodotoxin (TTX). These results suggest that the upper–lower and nasal-temporal asymmetries of PhNR in the primate retina are mainly caused by TTX-sensitive spiking activities of inner retinal neurons.

1. Introduction

The photopic negative response (PhNR) is a slow, negative-going wave of the photopic electroretinogram (ERG) that appears after the b-wave. Studies by Frishman and colleagues have demonstrated that the PhNR originates from the spiking activity of inner retinal neurons including the retinal ganglion cells and their axons (Rangaswamy et al., 2007; Viswanathan et al., 1999, 2000).The PhNR has been used in clinical studies to evaluate the inner retinal function objectively in several diseases, including glaucoma (Colotto et al., 2000; Drasdo et al., 2001; Machida et al., 2008; Viswanathan et al., 2001), optic nerve diseases (Gotoh et al., 2004; Miyata et al., 2007; Rangaswamy et al., 2004), and retinal vascular diseases (Chen et al., 2006; Kizawa et al., 2006; Machida et al., 2004). In these studies, the PhNRs were elicited mainly by full-field stimuli, and there have been only a few studies where the PhNR were elicited from localized retinal areas (Clotto et al., 2000; Fortune et al., 2003; Viswanathan et al., 2000). In addition, there have been only two studies of the focal PhNR with simultaneous fundus monitoring (Kondo et al., 2008; Machida et al., 2008).

We have recently developed a new recording system of focal PhNR (Kondo et al., 2008), which was modified from Miyake et al., 1988. In this system, the examiner can monitor the position of the stimulus spot on the fundus precisely during the recordings. In addition, a red stimulus spot was used on a blue background illumination, because a recent study showed that this color combination was most effective in eliciting large PhNRs especially for weak to moderate stimulus intensities (Rangaswamy et al., 2007). With this system, we found that the amplitude of the PhNR of the focal ERG was relatively large in the macular area (Kondo et al., 2008). However, we did not examine whether there were any regional variations or asymmetry in the amplitude of the PhNR in the macular area of monkeys. We believe that when the focal macular PhNRs are recorded from normal and diseased retinas, it is important to know whether there are any regional variations or asymmetries in the focal macular PhNR.

Thus, the purpose of this study was to determine whether the focal PhNRs recorded from the upper and lower macular areas, and nasal and temporal macular areas using a hemi-circular stimulus were symmetrical. We show that there were distinct asymmetries of the PhNR amplitude in both the vertical and horizontal directions in monkeys. We examined how these asymmetries of the focal PhNR change after the spiking activities of the inner retinal neurons are blocked by an intravitreal injection of tetrodotoxin (TTX) in monkeys.

2. Methods

2.1. Animals

Five eyes of five rhesus monkeys (*Macaca mulata*) were studied. The animals were sedated with an intramuscular injection of

* Corresponding author. Tel.: +81 52 744 2271; fax: +81 52 744 2278.
E-mail address: kondomi@med.nagoya-u.ac.jp (M. Kondo).

0014-4835/$ – see front matter © 2008 Elsevier Ltd. All rights reserved.
doi:10.1016/j.exer.2008.10.012

ketamine hydrochloride (7 mg/kg initial dose; 5–10 mg/kg per h maintenance dose) and xylazine (0.6 mg/kg). The respiration and heart rate were monitored, and hydration was maintained with slow infusion of lactated Ringer solution. The cornea was anesthetized with topical 1% tetracaine, and the pupils dilated with topical 0.5% tropicamide, 0.5% phenylephrine HCl, and 1% atropine. All experimental and animal care procedures adhered to the ARVO Statement for the Use of Animals in Ophthalmic and Vision Research, and were approved by the Institutional Animal Care Committee of the Nagoya University.

2.2. Stimulus and observation system

Our system for recording focal PhNRs has been described in detail (Kondo et al., 2008). Briefly, an infrared fundus camera was modified to observe the fundus and stimulate the retina. Light emitting diodes (LEDs) were incorporated into the camera to be used for the stimulus and background illuminations. The infrared television fundus camera (Kowa VX-10, Tokyo, Japan) was modified to obtain a Maxwellian stimulating system. The image from this fundus camera was fed to a television monitor with a 45° view of the posterior pole of the eye. The position of the stimulus spot on the fundus could be moved by the examiner with a joystick, and the position was monitored on the television monitor (Fig. 1, upper trace).

A red LED ($\lambda_{max} = 627$ nm; LXK2-PD12-S00, Philips Lumileds, San Jose, CA, USA) was used as the stimulus source, and a blue LED ($\lambda_{max} = 450$ nm; L450, Epitex, Kyoto, Japan) was used for the background illumination that covered a retinal area of 45°. A hemi-circular red stimulus (15° in diameter) was used (Fig. 1, lower trace).

The luminance of blue background was fixed at 100 scot cd/m^2, which is known to be high enough to suppress the rod photoreceptors. The luminance of the red stimulus spot was 55 phot cd/m^2, and the stimulus durations were 10 and 150 ms. We have already shown that the responses recorded with this system were focal when the luminance of the red stimulus spot was $\leq$55 phot cd/m^2 and presented on a steady blue background of 100 scot cd/m^2 (Kondo et al., 2008). The strength of the brief flashes of 10 ms was 0.55 phot cd-s/m^2 in energy units. The stimulus repetition rate was fixed at 2 Hz.

The luminances of the stimulus and background were measured at the position of corneal surface, and then converted to the value at the retinal surface. These luminances were measured with a photometer (Model IL 1700; International Light, Newburyport, MA, USA).

2.3. Recording and analyses

ERGs were picked-up with a Burian-Allen bipolar contact lens electrode (Hansen Ophthalmic Development Labs, Iowa City, USA), and the ground electrode was attached to the ipsilateral ear. The responses were amplified, and the band pass filters were set at 0.5 and 1000 Hz. The ERGs were digitized at 5 kHz, and 100– 300 responses were averaged for each response (MEB-9100, Neuropack, Nihon Kohden, Tokyo, Japan).

The amplitude of the PhNR was measured from the baseline to the bottom of the negative trough after the b-wave for the brief flashes of 10 ms, or was measured from the positive peak of the b-wave to the negative trough after the b-wave for the long duration

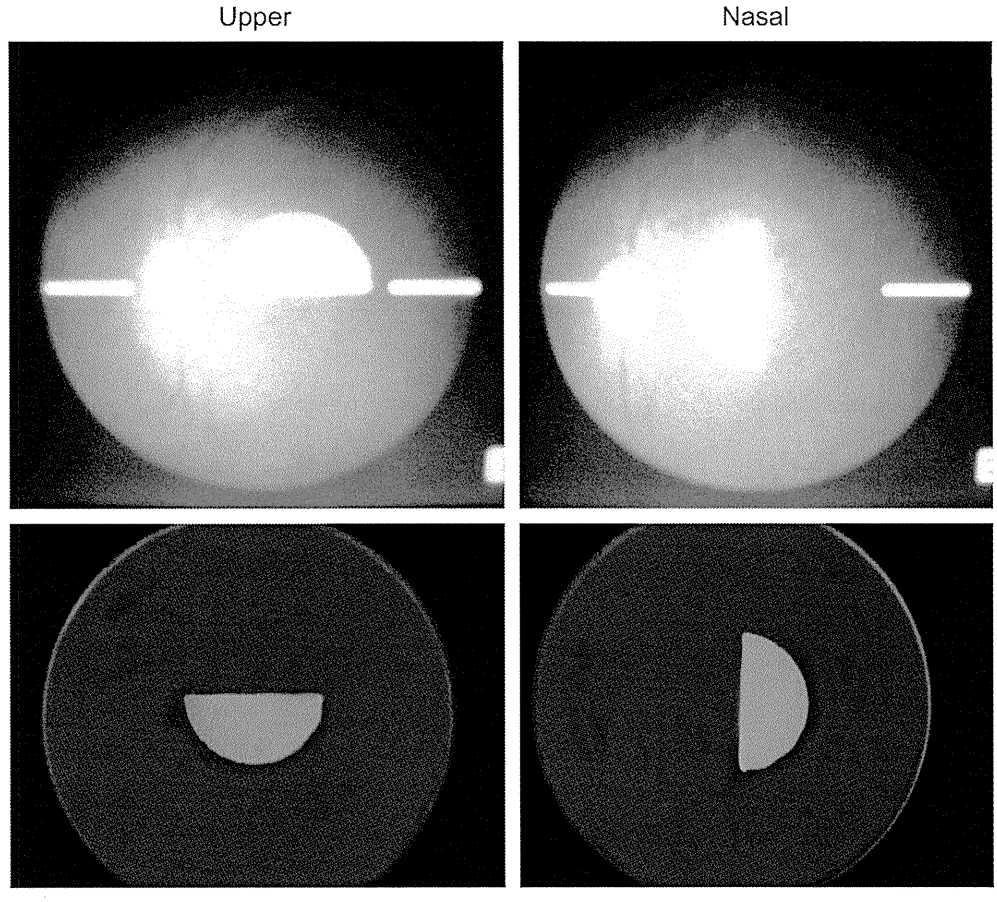

Fig. 1. Stimulus configuration for stimulating localized areas of the macula. Upper trace: Infrared fundus image of the monkey retina. The 15° hemi-circular stimulus is positioned on the upper (left) and nasal macula (right) of a rhesus monkey. Lower trace: Image of the red stimulus spot on the blue background. This image was photographed by a digital camera at the position of monkey's eye.

flashes of 150 ms as done in previous studies (Rangaswamy et al., 2007; Viswanathan et al., 1999). The amplitudes of the a- and b-waves were measured from the baseline to the first negative trough and from the negative trough to the next positive peak, respectively.

2.4. Injection of tetrodotoxin (TTX)

The intravitreal injection techniques have been described in detail (Hood et al., 1999; Kondo et al., 2008; Ueno et al., 2004, 2006; Viswanathan et al., 1999). The TTX was injected into the vitreous with a 30-gauge needle inserted through the pars plana approximately 3 mm posterior to the limbus. The TTX (Kanto Chemical, Tokyo Japan) was dissolved in sterile saline, and 0.05– 0.07 ml was injected. The intravitreal concentrations of TTX was 4 μM assuming that the monkey's vitreous volume is 2.1 ml.

Because the effect of TTX is maximal at about 60 min after the drug injection, recordings were begun about 60 min after the injections, and studies were completed within 3 h. The results that are shown were recorded from eyes not previously treated.

2.5. Statistical analyses

The data were analyzed with the Stat View ver.5 computer software. The amplitude of each ERG component (a-wave, b-wave, and PhNR) from the upper and lower macular areas, or from the nasal and temporal macular areas were compared using paired t -tests. A difference was considered statistically significant when $P < 0.05$.

3. Results

3.1. Asymmetry between upper and lower macular areas

Representative focal macular ERGs recorded from upper and lower macula areas in a rhesus monkey (monkey #4) are shown in Fig. 2A. The focal ERGs for brief-flashes (10 ms) and long-flashes (150 ms) are presented in the upper and lower traces, respectively. At first glance, the focal ERGs from the upper and lower macula areas appear nearly the same. But when the two waveforms were superimposed, the amplitude of the PhNR was slightly larger in the upper macular than in the lower macular areas for both brief and long duration stimuli (right most column of Fig. 2A).

The amplitudes of the PhNRs recorded from upper and lower macular areas for five different animals are plotted in Fig. 2B. The amplitudes from the upper macular area were larger than that recorded from the lower macular area in all five animals, although there was a large variation in the PhNR amplitude among the five animals. The mean (±SEM) PhNR amplitude of the upper macular area was 3.3 ± 0.4 μV which was 27% larger than that of lower macula at 2.6 ± 0.4 μV for brief-flashes ($P < 0.05$). Similarly, the mean (±SEM) PhNR amplitude of the upper retina was 5.4 ± 0.7 μV which was 20% larger than that of lower retina at 4.5 ± 0.5 μV for long duration stimuli ($P < 0.01$).

The mean (±SEM) of the amplitudes for the a-wave, b-wave, and PhNR are plotted in Fig. 2C. We noted that not only the PhNR amplitude, but also the a-wave amplitude was significantly larger in the upper macula than in the lower macula for brief-flashes ($P < 0.05$).

3.2. Asymmetry of PhNR recorded from nasal and temporal macular areas

Representative focal macular ERGs recorded from nasal and temporal retinas in the same monkey shown in Fig. 2A (monkey #4) are shown in Fig. 3A. We found that the amplitude of the PhNR recorded from the nasal macular area was slightly larger than the PhNR of temporal macular area for both brief and long duration stimuli in all five animals (Fig. 3B). For short duration stimuli, the mean (±SEM) PhNR amplitude of the nasal macular area was 3.3 ± 0.4 μV, which was 27% larger than that of temporal macular

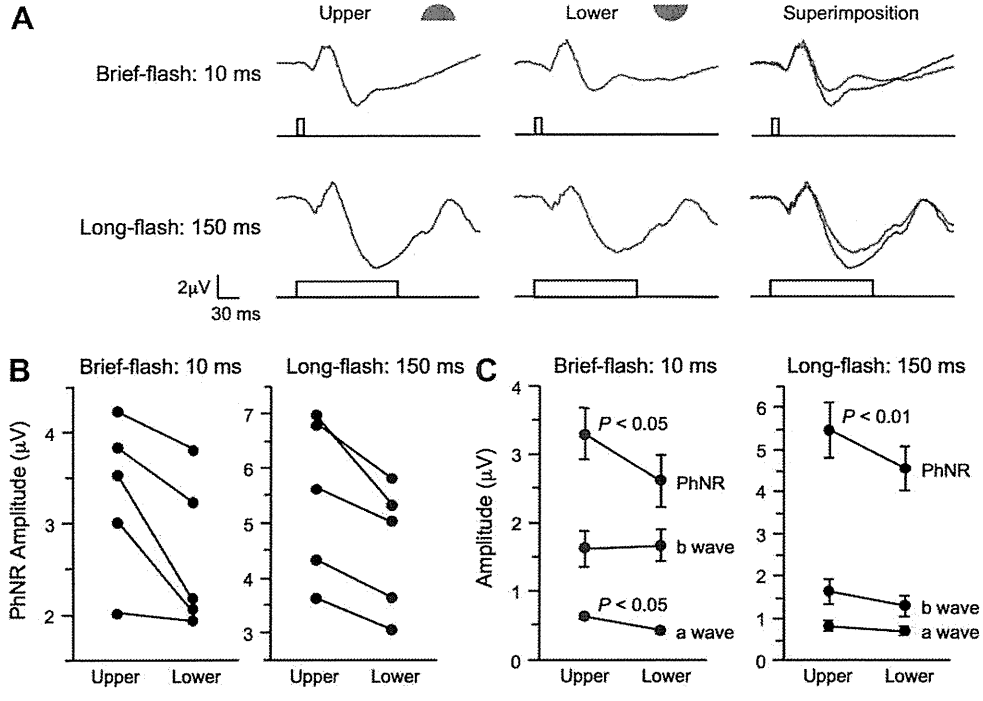

Fig. 2. Focal macular ERGs. (A) Representative focal macular ERGs recorded from the upper and lower macular areas in a rhesus monkey. ERGs for short duration (10 ms) and long duration (150 ms) stimuli are presented in the upper and lower traces, respectively. (B) Plot of the PhNR amplitude from five different monkeys. (C) Mean (±SEM) of the amplitudes for the a-wave, b-wave, and PhNR recorded from upper and lower macular areas for five monkeys. Note that the PhNR of upper macula is significantly larger than that of the lower macula.

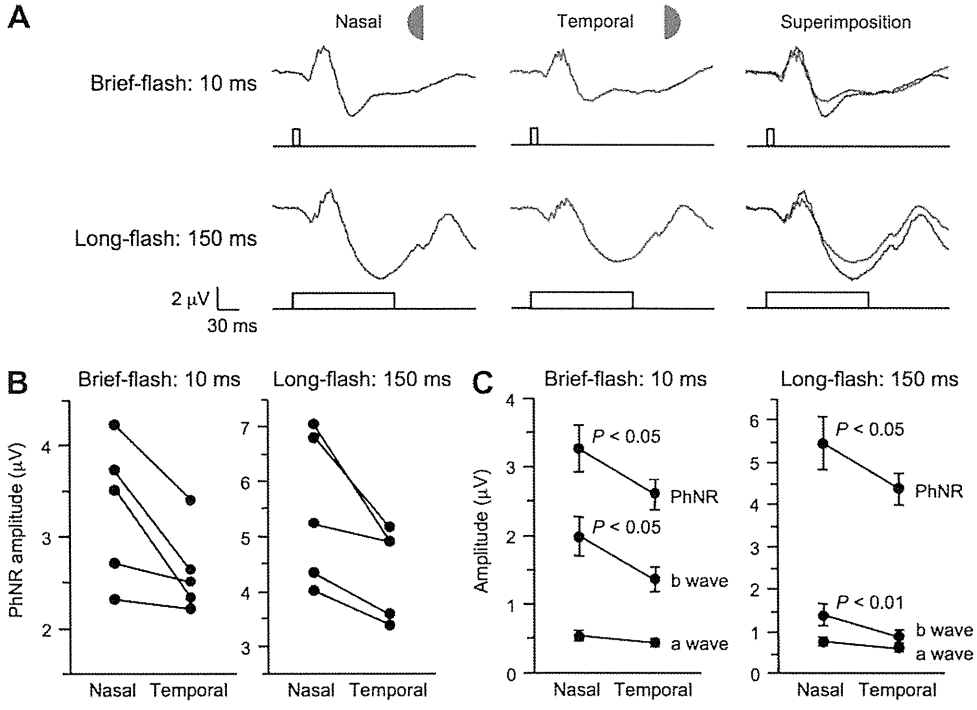

Fig. 3. Focal macular ERGs recorded from the nasal and temporal macular areas. (A) Representative focal macular ERGs recorded from nasal and temporal macular areas in a rhesus monkey. ERGs for short duration (10 ms) and long duration (150 ms) stimuli are presented in the upper and lower traces, respectively. (B) Plot of the PhNR amplitudes from five different monkeys. (C) Mean (±SEM) of the amplitudes for the a-wave, b-wave, and PhNR recorded from nasal and temporal maculae for five monkeys. Note that the PhNR of nasal macula is significantly larger than that of temporal macula.

area at 2.6 ± 0.2 μV. For long duration stimuli, the mean (±SEM) PhNR amplitude of the nasal macular area was 5.5 ± 0.6 μV which was 25% larger than that of temporal macular area at 4.4 ± 0.4 μV. All of these differences were statistically significant ($P < 0.05$).

The mean (±SEM) of the amplitudes for a-wave, b-wave, and PhNR are plotted in Fig. 3C. Not only the PhNR, but the b-wave was also significantly larger in the nasal macula than in the temporal macula for both short and long duration stimuli ($P < 0.05$).

3.3. Effect of TTX on upper–lower asymmetry

We next wanted to determine how TTX-sensitive neural activities contributed to the asymmetry of PhNR in monkeys. For this, we recorded the focal macular ERGs from different retinal locations before and after an intravitreal injection of TTX in two monkeys. Focal macular ERGs recorded from the upper and lower macular area before and after an intravitreous injection of TTX from a monkey (#4) are shown in Fig. 4A. As shown in Fig. 2, the PhNR amplitude was slightly larger in the upper macula than in the lower macula before the TTX injection (black waveforms). After the injection of TTX, the amplitudes of PhNR were greatly reduced for both short and long duration stimuli (blue and red waveforms).

The component removed by the TTX was isolated by subtracting the post-TTX response from the pre-TTX response (green and orange waveform). We found that the amplitude of TTX-sensitive negative component was 55 and 33% larger in the upper macula than in the lower macula for both short and long duration stimuli, respectively (third column from the left). In another monkey (monkey #5), the amplitude of this TTX-sensitive negative component was 35 and 23% larger in the upper macular area than in the lower macular area for both brief and long-flashes, respectively (Fig. 4B).

Interestingly, waveforms of the remaining ERGs after TTX from upper and lower areas became identical (second column from the left of Fig. 4A). This was also true for another animal (monkey #5, blue and red waveforms of Fig. 4B).

3.4. Effect of TTX on nasal-temporal asymmetry

We also studied the effect of TTX on the nasal-temporal asymmetry of the PhNR in two monkeys. Focal macular ERGs recorded from the nasal and temporal macular areas before and after intravitreal TTX injection (monkey #4) are shown in Fig. 5A. As in Fig. 4, the amplitudes of PhNR were greatly reduced after the TTX injection for both short and long duration stimuli.

The component removed by TTX was isolated by subtracting the post-TTX response from the pre-TTX response. We found that the amplitude of the TTX-sensitive negative component was 42 and 31% larger in the nasal macula than in the temporal macula for both short and long duration stimuli, respectively (third column from the left). In another monkey (monkey #5), the amplitude of TTX-sensitive negative component was 23 and 22% larger in the nasal macula than in the temporal macula for both sort and long duration stimuli, respectively (Fig. 5B).

Again, waveforms of the remaining ERGs after TTX from nasal and temporal areas became identical (second column from the left of Fig. 5A), and overlapped for two monkeys (second column from the left of Fig. 5A, and blue and red waveforms of Fig. 5B).

4. Discussion

Our results demonstrated that there were significant asymmetries in the amplitude of PhNR in the macular area of monkeys. The PhNR of upper macula was larger than that of lower macula, and the PhNR of nasal macula was larger than that of temporal macula. These asymmetries of the PhNR were present for both short and long duration stimuli. The degree of the differences in the PhNR amplitude was dependent on the stimulus duration and locations, and ranged from 20 to 27% for the stimuli used in this study. To the

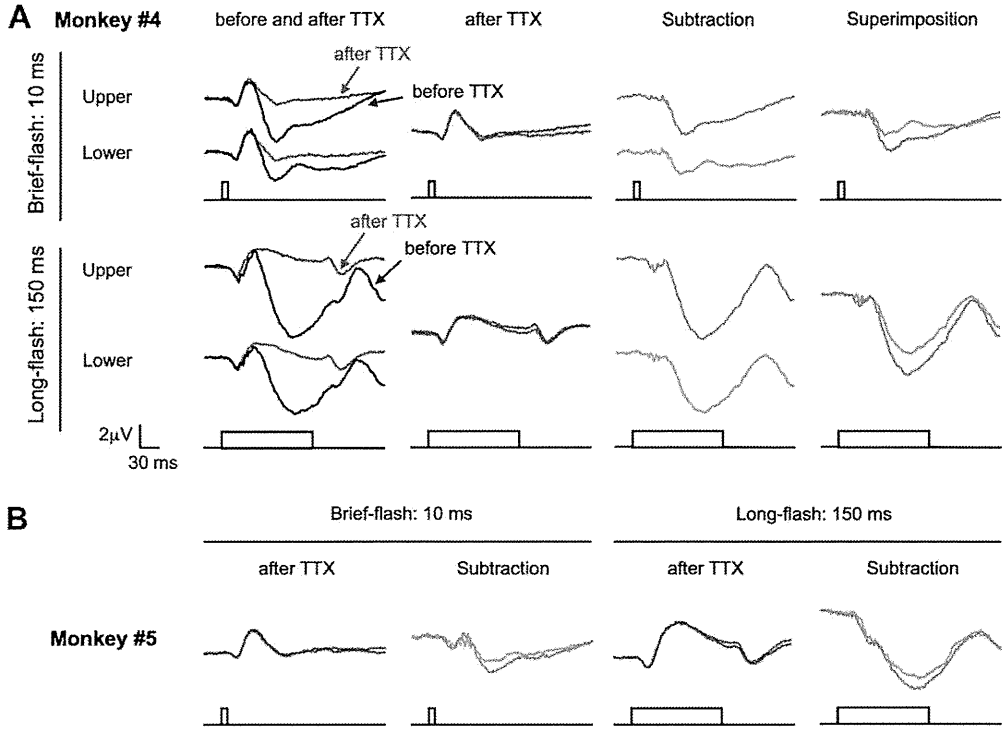

Fig. 4. Effect of tetrodotoxin (TTX) on the PhNR. (A) Representative focal ERGs recorded from the upper and lower macular areas before and after an intravitreal injection of TTX in a monkey (#4). ERGs elicited by short duration stimuli are shown in the upper trace, and ERGs elicited by long duration stimuli are shown in the lower traces. Subtracted TTX-sensitive components are also shown in the third and fourth rows from the left. (B) Results from another monkey (#5). Waveforms after TTX and subtracted TTX-sensitive components from upper and lower maculae are superimposed.

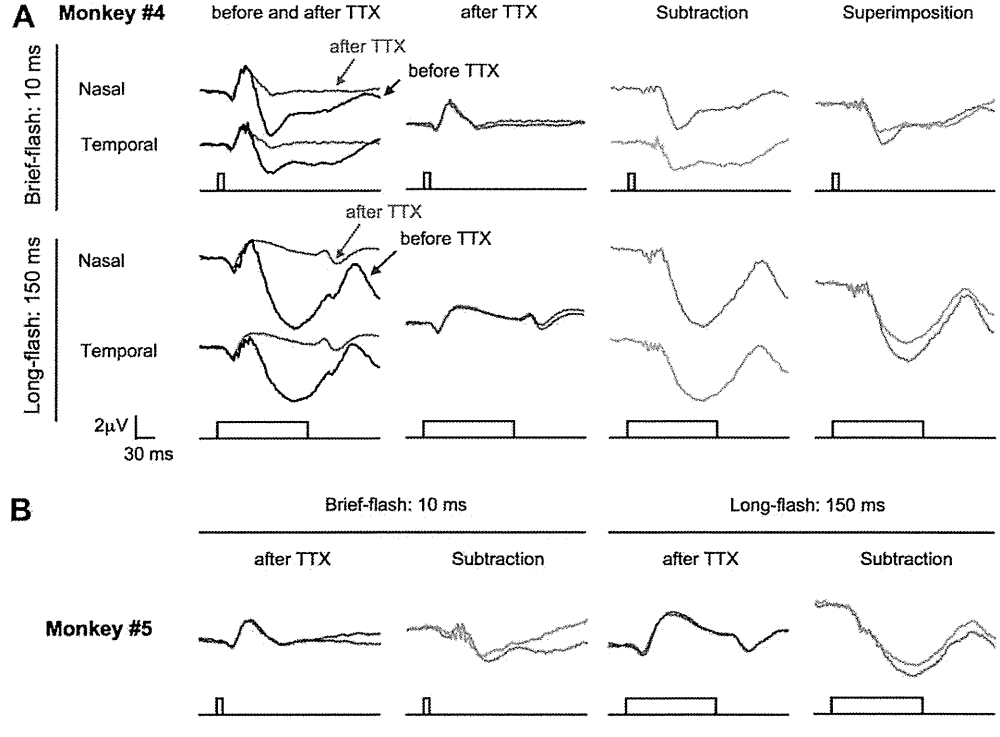

Fig. 5. Effect of tetrodotoxin (TTX) on the PhNR. (A) Representative focal ERGs recorded from the nasal and temporal macular areas before and after intravitreal injection of TTX in monkey #4. The ERGs to short duration stimuli are shown in the upper traces, and ERGs to long duration stimuli are shown in the lower traces. The subtracted TTX-sensitive components are shown in the third and fourth rows from the left. (B) Results from another monkey (#5). Waveforms after TTX and subtracted TTX-sensitive components from nasal and temporal maculae are superimposed.

best of our knowledge, this is the first demonstration that there is upper–lower and nasal-temporal asymmetries of the PhNR amplitudes in primates.

The asymmetries in the amplitudes were observed not only in the PhNR but also in the a- and b-waves of the focal macular ERGs (Figs. 2 and 3). One question then arises as to whether the larger PhNRs in the superior and nasal macular areas may be due to the larger signal inputs transmitted to the inner retina. To exclude this possibility, we blocked the spiking activities of inner retinal neurons by intravitreal injection of TTX. The results showed that after TTX, there was no apparent asymmetry in the waveforms of focal macular ERGs between the superior and inferior macular areas, and between nasal and temporal macular areas (Figs. 4 and 5). In contrast, subtracted TTX-sensitive components showed distinct upper–lower and nasal-temporal asymmetries. These findings were consistent for the two different monkeys tested. These results suggested that the larger PhNRs at the upper and nasal macular areas were not due to the larger signal inputs transmitted to the inner retinal neurons, but were mainly caused by TTX-sensitive spiking activity of inner retinal neurons.

Our results of asymmetry in the PhNR amplitude are in agreement with previous histological studies in humans (Curcio and Allen, 1990) and monkeys (Perry and Cowey, 1985; Silveira et al., 1989, 1993). They reported that the ganglion cell density of the upper retina is higher than that of lower retina, and ganglion cell density of nasal retina was higher than that of the temporal retina, including macular area. Curcio and Allen (1990) reported that the ganglion cell density is about 15% higher in the nasal retina than at equivalent eccentricities in temporal retina from 0.4 to 2.0 mm eccentricity in human retinas. They also found that the ganglion cell density is approximately equal between upper and lower retinas at the eccentricities of 0.4 –2 mm, but the upper retina has 65% higher ganglion cell density than inferior retina at eccentricities of 2 –4 mm. When we consider the size of a stimulus spot of 15°, which corresponds to a retinal area of 2.8– 3.0 mm from the fovea, it is reasonable to interpret that the asymmetry of PhNR amplitude found in this study was mainly caused by the asymmetry of ganglion cell density.

Our results are also in agreement with other electrophysiological studies. The amplitude of pattern ERG, which is also thought to reflect the activity of ganglion cells and axons (Baker et al., 1988; Maffei and Fiorentini, 1981; Maffei et al., 1985), was larger in the upper retina than in the lower retina (Graham et al., 1994; Yoshii and Päärmann, 1989). In addition, the amplitude of the pattern ERG was greater in the nasal retina than in the temporal retina (Bopp, 1982; Porrello and Falsini, 1999; Yoshii and Päärmann, 1989). These findings combined with a recent study comparing the PhNR and pattern ERG in monkeys (Viswanathan et al., 2000) supported the idea that the PhNR and pattern ERG may be of similar cellular origin.

It is known that another inner retinal ERG component, the oscillatory potentials (OPs), shows a distinct nasal-temporal asymmetry in the retina of humans (Bearse et al., 2000; Miyake et al., 1989; Wu and Sutter, 1995) and monkeys (Rangaswamy et al., 2003, 2006). In contrast to PhNR, the OPs are larger in the temporal retina than in the nasal retina. Recent studies found that this nasal-temporal asymmetry of OPs was greatly reduced in monkeys after an intravitreal injection of TTX (Rangaswamy et al., 2003), monkeys with experimental glaucoma (Rangaswamy et al., 2006), and patients with glaucoma (Fortune et al., 2002). This nasal-temporal asymmetry in OPs is thought to be related to summation or subtraction of an optic nerve head component (ONHC) with local retinal component, depending upon the distance of the local region stimulated from the optic nerve head (Bearse et al., 2000; Zhou et al., 2007).

Hood et al. (1999) also studied the variation in the waveforms of fast multifocal ERG in rhesus monkeys. They found that intravitreal injection of TTX eliminated the variation and asymmetry in the waveforms of fast multifocal ERG across the retina. From these results, they suggested that the waveform variation and asymmetry in the fast multifocal ERG are mainly caused by TTX-sensitive inner retinal neurons.

What is the clinical relevance of this study? The focal PhNR has been used to assess inner retinal function of local areas in clinical situations (Drasdo et al., 2001; Machida et al., 2008). In the clinic, the focal PhNR may be separately recorded from upper and lower retinas, or from nasal and temporal retinas in patients with optic nerve diseases or glaucoma. In such occasions, it is important to remember that there are asymmetries in the PhNR amplitude in normal subjects. Furthermore, investigations are needed to study how local PhNRs are affected and how the asymmetry of PhNR changes in clinical diseases.

Acknowledgements

We thank Professor Yozo Miyake of Shukutoku University and Professor Duco I. Hamasaki for discussions on the manuscript. We also thank Mr Masao Yoshikawa, Hideteka Kudo, and Ei-ichiro Nagasaka of Mayo Corporation for technical help. Grant support: Health Sciences Research Grants (H16-sensory-001) from the Ministry of Health, Labor and Welfare, Japan, and Ministry of Education, Culture, Science and Technology (no. 18591913 and 18390466). The authors have no proprietary interests.

References

Baker Jr., C.L., Hess, R.R., Olsen, B.T., Zrenner, E., 1988. Current source density analysis of linear and non-linear components of the primate electroretinogram. J. Physiol. 407, 155–176.

Bearse Jr., M.A., Shimada, Y., Sutter, E.E., 2000. Distribution of oscillatory components in the central retina. Doc. Ophthalmol. 100, 185–205.

Bopp, M., 1982. Predominance of the nasal hemiretina in the pattern electroretinogram of the human eye. Pflügers Arch. 392, 50.

Chen, H., Wu, D., Huang, S., Yan, H., 2006. The photopic negative response of the flash electroretinogram in retinal vein occlusion. Doc. Ophthalmol. 113, 53–59.

Colotto, A., Falsini, B., Salgarello, T., Iarossi, G., Galan, M.E., Scullica, L., 2000. Photopic negative response of the human ERG: losses associated with glaucomatous damage. Invest. Ophthalmol. Vis. Sci. 41, 2205–2211.

Curcio, C.A., Allen, K.A., 1990. Topography of ganglion cells in human retina. J. Comp. Neurol. 300, 5–25.

Drasdo, N., Aldebasi, Y.H., Chiti, Z., Mortlock, K.E., Morgan, J.E., North, R.V., 2001. The S-cone PhNR and pattern ERG in primary open angle glaucoma. Invest. Ophthalmol. Vis. Sci. 42, 1266–1272.

Fortune, B., Bearse Jr., M.A., Cioffi, G.A., Johnson, C.A., 2002. Selective loss of an oscillatory component from temporal retinal multifocal ERG responses in glaucoma. Invest. Ophthalmol. Vis. Sci. 43, 2638–2647.

Fortune, B., Wang, L., Bui, B.V., Cull, G., Dong, J., Cioffi, G.A., 2003. Local ganglion cell contributions to the macaque electroretinogram revealed by experimental nerve fiber layer bundle defect. Invest. Ophthalmol. Vis. Sci. 44, 4567–4579.

Gotoh, Y., Machida, S., Tazawa, Y., 2004. Selective loss of the photopic negative response in patients with optic nerve atrophy. Arch. Ophthalmol. 122, 341–346.

Graham, S.L., Wong, V.A., Drance, S.M., Mikelberg, F.S., 1994. Pattern electroretinograms from hemifields in normal subjects and patients with glaucoma. Invest. Ophthalmol. Vis. Sci. 35, 3347–3356.

Hood, D.C., Frishman, L.J., Viswanathan, S., Robson, J.G., Ahmed, J., 1999. Evidence for a ganglion cell contribution to the primate electroretinogram (ERG): effects of TTX on the multifocal ERG in macaque. Vis. Neurosci. 16, 411–416.

Kizawa, J., Machida, S., Kobayashi, T., Gotoh, Y., Kurosaka, D., 2006. Changes of oscillatory potentials and photopic negative response in patients with early diabetic retinopathy. Jpn. J. Ophthalmol. 50, 367–373.

Kondo, M., Kurimoto, Y., Sakai, T., Koyasu, T., Miyata, K., Ueno, S., Terasaki, H., 2008. Recording focal macular photopic negative response (PhNR) from monkeys. Invest. Ophthalmol. Vis. Sci. 49, 3544–3550.

Machida, S., Gotoh, Y., Tanaka, M., Tazawa, Y., 2004. Predominant loss of the photopic negative response in central retinal artery occlusion. Am. J. Ophthalmol. 137, 938–940.

Machida, S., Toba, Y., Ohtaki, A., Gotoh, Y., Kaneko, M., Kurosaka, D., 2008. Photopic negative response of focal electoretinograms in glaucomatous eyes. Invest. Ophthalmol. Vis. Sci. [Epub ahead of print].

Maffei, L., Fiorentini, A., 1981. Electroretinographic responses to alternating gratings before and after section of the optic nerve. Science 211, 953–955.

Maffei, L., Fiorentini, A., Bisti, S., Holländer, H., 1985. Pattern ERG in the monkey after section of the optic nerve. Exp. Brain. Res. 59, 423–425.

Miyake, Y., Shiroyama, N., Ota, I., Horiguchi, M., 1988. Oscillatory potentials in electroretinograms of the human macular region. Invest. Ophthalmol. Vis. Sci. 29, 1631–1635.

Miyake, Y., Shiroyama, N., Horiguchi, M., Ota, I., 1989. Asymmetry of focal ERG in human macular region. Invest. Ophthalmol. Vis. Sci. 30, 1743–1749.

Miyata, K., Nakamura, M., Kondo, M., Lin, J., Ueno, S., Miyake, Y., Terasaki, H., 2007. Reduction of oscillatory potentials and photopic negative response in patients with autosomal dominant optic atrophy with OPA1 mutations. Invest. Ophthalmol. Vis. Sci. 48, 820–824.

Perry, V.H., Cowey, A., 1985. The ganglion cell and cone distributions in the monkey's retina: implications for central magnification factors. Vision Res. 25, 1795–1810.

Porrello, G., Falsini, B., 1999. Retinal ganglion cell dysfunction in humans following post-geniculate lesions: specific spatio-temporal losses revealed by pattern ERG. Vision Res. 39, 1739–1745.

Rangaswamy, N.V., Hood, D.C., Frishman, L.J., 2003. Regional variations in local contributions to the primate photopic flash ERG: revealed using the slow-sequence mfERG. Invest. Ophthalmol. Vis. Sci. 44, 3233–3247.

Rangaswamy, N.V., Frishman, L.J., Dorotheo, E.U., Schiffman, J.S., Bahrani, H.M., Tang, R.A., 2004. Photopic ERGs in patients with optic neuropathies: comparison with primate ERGs after pharmacologic blockade of inner retina. Invest. Ophthalmol. Vis. Sci. 45, 3827–3837.

Rangaswamy, N.V., Shirato, S., Kaneko, M., Digby, B.I., Robson, J.G., Frishman, L.J., 2007. Effects of spectral characteristics of Ganzfeld stimuli on the photopic negative response (PhNR) of the ERG. Invest. Ophthalmol. Vis. Sci. 48, 4818–4828.

Rangaswamy, N.V., Zhou, W., Harwerth, R.S., Frishman, L.J., 2006. Effect of experimental glaucoma in primates on oscillatory potentials of the slow-sequence mfERG. Invest. Ophthalmol. Vis. Sci. 47, 753–767.

Silveira, L.C., Picanço-Diniz, C.W., Sampaio, L.F., Oswaldo-Cruz, E., 1989. Retinal ganglion cell distribution in the cebus monkey: a comparison with the cortical magnification factors. Vision Res. 29, 1471–1483.

Silveira, L.C., Perry, V.H., Yamada, E.S., 1993. The retinal ganglion cell distribution and the representation of the visual field in area 17 of the owl monkey, *Aotus trivirgatus*. Vis. Neurosci. 10, 887–897.

Ueno, S., Kondo, M., Niwa, Y., Terasaki, H., Miyake, Y., 2004. Luminance dependence of neural components that underlies the primate photopic electroretinogram. Invest. Ophthalmol. Vis. Sci. 45, 1033–1040.

Ueno, S., Kondo, M., Ueno, M., Miyata, K., Terasaki, H., Miyake, Y., 2006. Contribution of retinal neurons to d-wave of primate photopic electroretinograms. Vision Res. 46, 658–664.

Viswanathan, S., Frishman, L.J., Robson, J.G., Harwerth, R.S., Smith III, E.L., 1999. The photopic negative response of the macaque electroretinogram: reduction by experimental glaucoma. Invest. Ophthalmol. Vis. Sci. 40, 1124–1136.

Viswanathan, S., Frishman, L.J., Robson, J.G., 2000. The uniform field and pattern ERG in macaques with experimental glaucoma: removal of spiking activity. Invest. Ophthalmol. Vis. Sci. 41, 2797–2810.

Viswanathan, S., Frishman, L.J., Robson, J.G., Walters, J.W., 2001. The photopic negative response of the flash electroretinogram in primary open angle glaucoma. Invest. Ophthalmol. Vis. Sci. 42, 514–522.

Wu, S., Sutter, E.E., 1995. A topographic study of oscillatory potentials in man. Vis. Neurosci. 12, 1013–1025.

Yoshii, M., Päärmann, A., 1989. Hemiretinal stimuli elicit different amplitudes in the pattern electroretinogram. Doc. Ophthalmol. 72, 21–30.

Zhou, W., Rangaswamy, N., Ktonas, P., Frishman, L.J., 2007. Oscillatory potentials of the slow-sequence multifocal ERG in primates extracted using the Matching Pursuit method. Vision Res. 47, 2021–2036.

CONCENTRATION OF VASCULAR ENDOTHELIAL GROWTH FACTOR IN AQUEOUS HUMOR OF EYES WITH ADVANCED RETINOPATHY OF PREMATURITY BEFORE AND AFTER INTRAVITREAL INJECTION OF BEVACIZUMAB

NORIE ITO NONOBE, MD, SHU KACHI, MD, PHD, MINEO KONDO, MD, PHD, YOSHIKO TAKAI, MD, PHD, KOJI TAKEMOTO, MD, ATSUSHI NAKAYAMA, MD, MASAHIRO HAYAKAWA, MD, PHD, HIROKO TERASAKI, MD, PHD

Purpose: To determine whether an intravitreal injection of bevacizumab alters the concentration of vascular endothelial growth factor (VEGF) in the aqueous humor of eyes with retinopathy of prematurity.

Methods: Seven Stage 4 and three Stage 5 eyes of eight patients with retinopathy of prematurity were studied. Bevacizumab (0.75 mg/0.03 mL/eye) was injected intravitreally in six eyes of six patients after approval was obtained from the Institutional Review Board of Nagoya University Hospital and an informed consent was signed by the parents. Aqueous humor was collected just before the surgery or before the intravitreal injection of bevacizumab. Aqueous humor was also collected immediately before vitrectomy 4 to 48 days after the injection of bevacizumab. Aqueous humor was also collected from four patients undergoing congenital cataract surgery as controls. The concentration of VEGF was measured by enzyme-linked immunosorbent assay.

Results: In the 4 control eyes, the concentration of VEGF in 2 eyes was 156 and 158 pg/mL and was not detectable in the other 2 eyes. The average concentration of VEGF was 1,109 pg/mL in the active Stage 4 eyes and 3,520 pg/mL in the active Stage 5 eyes. After bevacizumab injection, the unbound VEGF concentration was 60, 230, and 290 pg/mL in 3 eyes and not detectable in 1 eye.

Conclusion: Intravitreal bevacizumab resulted in a marked decrease in the unbound VEGF concentration in eyes with retinopathy of prematurity.

RETINA 29:579–585, 2009

Vascular endothelial growth factor (VEGF) is a dimeric glycoprotein that plays an important role in angiogenesis and neovascularization.[1] The retina is known to be ischemic in certain ocular diseases, such as diabetic retinopathy and retinopathy of prematurity (ROP), and the expression of VEGF is up-regulated, which leads to retinal neovascularization. This is important because the neovascularization can progress to vitreous hemorrhage, proliferative membranes, and retinal detachments (RDs).[2–4] Thus, one of the strategies to prevent these vision-threatening changes is to block the upregulation of VEGF.

From the Department of Ophthalmology, Nagoya University Graduate School of Medicine, Tsurumai, Showa-ku, Nagoya, Japan.

Grant-in-Aid for Scientific Research from the Ministry of Education, Culture, Sports, Science, and Technology of Japan [19791262 (S.K.), 18390466 (H.T.)].

Reprint requests: Hiroko Terasaki, MD, PhD, Department of Ophthalmology, Nagoya University Graduate School of Medicine, 65 Tsurumai, Showa-ku, Nagoya 466-8550, Japan; e-mail: terasaki@med.nagoya-u.ac.jp

Bevacizumab (Avastin; Genentech Inc., San Francisco, CA) is a humanized anti-VEGF monoclonal antibody that has been used systemically to treat patients with cancer.[5] For the eye, an intravitreal injection of bevacizumab was found to be effective in reducing the severity of ocular diseases such as neovascular age-related macular degeneration,[6] retinal vein occlusion,[7] and diabetic retinopathy.[8] Bevacizumab has also been used as a preoperative adjunctive therapy for proliferative diabetic retinopathy (PDR).[9] Sawada et al[10] have reported a marked decrease of ocular unbound VEGF level after an intravitreal injection of bevacizumab in eyes with PDR suggesting that the effectiveness of bevacizumab was due to a reduction of the unbound VEGF level.

ROP is a major cause of serious visual impairment in infants born prematurely, and the number of cases of severe ROP is increasing with the increase in the survival rate of the smallest pronatis.[11] In most cases, retinal photocoagulation is very effective in treating eyes with ROP, and the photocoagulation leads to a quiescent stage. However, despite this treatment, some eyes progress to the advanced stages of ROP with proliferative membranes and RDs. For severe cases, vitrectomy must be performed to reattach the retina, although surgeons must wait for the neovascular membranes to become quiescent, which greatly hinders the prognosis of good vision.

VEGF plays a key role in progression of ROPs, and Chung et al[12] have reported that bevacizumab was effective in treating eyes with ROP. This finding suggested that preoperative bevacizumab can be an effective adjunctive therapy for ROP. To the best of our knowledge, there have been only two studies on the ocular VEGF level in eyes with ROP,[13,14] and neither of these reported the level of VEGF after an intravitreal injection of bevacizumab.

Thus, the purpose of this study was to measure the concentration of VEGF in the aqueous humor in eyes with Stage 4 and Stage 5 ROP before and after an intravitreal injection of bevacizumab.

Methods

Subjects

Approval for this study was obtained from the Institutional Review Board of Nagoya University Hospital, and an informed consent was obtained from the parents. The procedures used in this study conformed to the tenets of the Declaration of Helsinki.

Seven eyes at Stage 4 and three at Stage 5 of eight patients with ROP were studied (Table 1). The mean postmenstrual age of the patients was 41.1 weeks (35–64 weeks). Bevacizumab at a dosage of 0.75 mg/0.03 mL was injected intravitreally in 6 eyes of 6 patients. An encircling or buckling procedure was performed on four eyes at Stage 4 ROP. Vitrectomy with lensectomy was performed on two Stage 4B and on two Stage 5 ROP eyes after bevacizumab injection, and in one Stage 5 ROP eye without an injection.

Aqueous humor was collected just before the surgery from seven eyes at Stage 4 and three at Stage 5 eyes. Aqueous humor was also collected just before the intravitreal injection of bevacizumab from two eyes at Stage 4 and two at Stage 5. For control, aqueous humor was also collected from three eyes with congenital cataract and one eye with persistent pupillary membrane that underwent surgery (1 male and 3 female infants). The mean age of these patients was 4.0 ± 2.1 months with a range of 2 to 7 months. Ophthalmoscopy showed that the fundus was normal in these four eyes. Although the eyes used as control were younger than that used in a previous report,[14] they were still older than the ROP eyes. This difference in the ages might have altered the VEGF level.

Ophthalmologic Examinations and Staging of Retinopathy of Prematurity

Fundus and 15-MHz ultrasound biomicroscopy (RION Inc., Kokubunji, Tokyo) examinations were performed on all eyes in the outpatient clinic. Color fundus photographs were taken with RetCam (Massie Research Laboratories Inc., Dublin, CA). Fluorescein angiography was performed under general anesthesia using the fluorescein angiography unit of the RetCam just before the sample collection.

The stage of the ROP was classified according to international classification,[15] and the vascular activity was classified as active if the eye had 1) plus disease, 2) new vessels growing into the vitreous at the ridge of a tractional RD area, or 3) combined effusive and tractional RD.[14]

Sample Collection and Measurement of Vascular Endothelial Growth Factor

Aqueous humor was collected under general anesthesia with a 27-gauge needle just before the surgery or intravitreal injection of bevacizumab. The amount of undiluted aqueous humor collected ranged from 0.02 mL to 0.1 mL. The samples were not analyzed at the time of collection, but were stored in a deep freezer at −80°C until use. The concentration of VEGF was measured by enzyme-linked immunosorbent assay using a commercially available kit (Quantikine: R&D Systems Inc., Minneapolis, MN), which measures both human $VEGF_{121}$ and $VEGF_{165}$. There

Table 1. Patient Characteristics and the Concentration of VEGF in Aqueous Humor

Patient No.	Gestational Age (Weeks)	Postmenstrual Age (Weeks)	Age (Months)	VEGF Before or Without Bevacizumab (pg/mL)	VEGF After Bevacizumab (pg/mL)
Control					
1			2	156	
2			2	ND	
3			5	ND	
4			7	158	
Stage 4 ROP					
1	22	39		564	
2	26	37		944	
3R	27	37		1,750	
3L	27	37		1,890	
4*	24	64		184	
5	25	41†			60 (4 days‡)
6	22	35, 36†		395	ND (4 days‡)
Stage 5 ROP					
7	28	40, 41†		1,990	230 (7 days‡)
8L	23	36, 43†		5,050	290 (48 days‡)
8R*	23	45		370	

*Inactive.
†Postmenstrual age when aqueous humor was collected after bevacizumab injection.
‡Days after bevacizumab injection.
ND, not detectable.

were three samples in which the VEGF was not detectable. However, as the amount of the samples collected from each eye was different and less than 0.2 mL, the minimum amount necessary for the test, all of the samples had to be diluted with Calibrator Diluent RD6U before use. The sample from Control 2 was diluted 10×, Control 3 was diluted 4×, and ROP 6 after bevacizumab was diluted 5× before the measurement. Thus, the concentration of VEGF in these eyes, in which VEGF was not detectable, might have been higher than 31 pg/mL, the minimum detectable limit of this kit.

Results

The concentration of VEGF in the aqueous humor of 1 of the eyes with congenital cataract was 158 pg/mL, and it was less than the detection level in the other 2 eyes. The concentration in an eye with a persistent pupillary membrane was 156 pg/mL.

The concentration of VEGF in 10 eyes with ROP ranged from 184 to 5,050 pg/mL, which is approximately 1.2× to 32× higher than that in the control eyes (Figure 1). Aqueous humor was collected from seven eyes at Stage 4 and three eyes at Stage 5. One eye at Stage 4 and one at Stage 5 were vascularly inactive. The mean concentration of VEGF in the vascularly active ROP was 1,109 pg/mL in the 5 Stage 4 eyes (395, 564, 944, 1,750, and 1,890 pg/mL in the Stage 4 eyes), and 3,520 pg/mL in the 2 Stage 5 eyes (1,990 and 5,050 pg/mL). In the vascularly inactive eyes, the VEGF level was 184 pg/mL in the 1 Stage 4 eye and 370 pg/mL in 1 Stage 5 eye. Thus, the concentration of VEGF in the vascularly active eyes tended to be higher than in inactive eyes, although statistical analysis could not be performed due to the small number of eyes (Figure 1).

Bevacizumab was injected into six active ROP eyes, four at Stage 4 and two at Stage 5, and aqueous humor was collected from two Stage 4 and two Stage 5 eyes 4 to 48 days after the injection just before vitrectomy. In the Stage 4 eyes, the concentration of

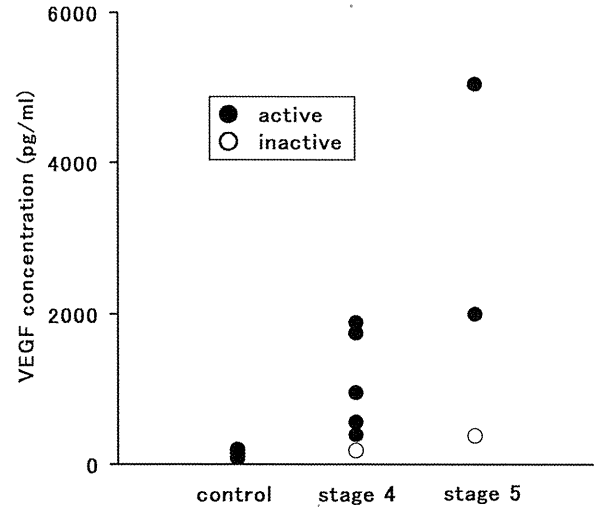

Fig. 1. Concentration of vascular endothelial growth factor (VEGF) in the aqueous humor without or before bevacizumab injection in Stages 4 and 5 ROP and control eyes are shown.